Research Square

Preprints are preliminary reports that have not undergone peer review.
They should not be considered conclusive, used to inform clinical practice,
or referenced by the media as validated information.

Genome-wide association study in Arabidopsis reveals IAN genes regulate pollen heatwave tolerance

Max Frencken
Radboud University
Daan M. van den Brink
Radboud University
Jeroen van den Hurk
Radboud University
Lotte van der Krabben
Radboud University
Elise A.R. Serin
Genetwister Technologies B.V.
Ivo Rieu
ivo.rieu@ru.nl

Radboud University

Research Article

Keywords: Arabidopsis thaliana, pollen thermotolerance, heatwave, genome-wide association study (GWAS), image analysis, IAN genes

Posted Date: October 29th, 2026

DOI: https://doi.org/10.21203/rs.3.rs-11319537/v1

License: This work is licensed under a Creative Commons Attribution 4.0 International License.
Read Full License

Additional Declarations: Competing interest reported. This work was funded by the Dutch Research Council (NWO; grant number 18039, to Ivo Rieu).

Genome-wide association study in Arabidopsis reveals IAN genes regulate pollen heatwave tolerance

Authors

Max Frencken; Dept of Plant & Animal Biology, Radboud Institute for Biological and Environmental Sciences, Radboud University, Nijmegen, The Netherlands; max.frencken@ru.nl

Daan M. van den Brink; Dept of Plant & Animal Biology, Radboud Institute for Biological and Environmental Sciences, Radboud University, Nijmegen, The Netherlands; daan.vandenbrink@ru.nl;

Jeroen van den Hurk; Dept of Plant & Animal Biology, Radboud Institute for Biological and Environmental Sciences, Radboud University, Nijmegen, The Netherlands; pjjhurk@hotmail.com

Lotte van der Krabben; Dept of Plant & Animal Biology, Radboud Institute for Biological and Environmental Sciences, Radboud University, Nijmegen, The Netherlands; lotte.vanderkrabben@ru.nl

Elise A.R Serin; Genetwister Technologies B.V., Wageningen, The Netherlands; E.Serin@genetwister.nl

Ivo Rieu (**corresponding author**); Dept of Plant & Animal Biology, Radboud Institute for Biological and Environmental Sciences, Radboud University, Nijmegen, The Netherlands; ivo.rieu@ru.nl

Acknowledgements

We thank N. van Bers, E. Iniesto, L. Rojas Martinez, F. Lanfenmeijer, G. van den Bunt, P. Kuin, D. Fleury and M. de Vos for their advice and insights, the staff of the Radboud University Experimental Garden and Genebank (Nijmegen, The Netherlands) for their assistance in plant cultivation, L. Vos, N. van der Wal and D. Hastabrata for experimental support, C. Alonso-Blanco for sharing with us the SNP dataset for genetic analysis, and S. Liu and J. Hua for providing the *IAN* KO-mutants. We acknowledge Genetwister Technologies B.V. for their support in performing statistical analyses and Copernicus Climate Change Service, and the data providers in the ECA&D project (https://www.ecad.eu) for the E-OBS dataset from the EU-FP6 project UERRA (https://www.uerra.eu).

Key Message

A machine learning-based pollen viability assay enabled GWAS and functional validation of IAN genes as negative regulators of pollen heatwave tolerance in *Arabidopsis thaliana*.

Abstract

Pollen development is highly sensitive to heatwave conditions in many plant species. Oftentimes, heatwave-induced pollen abortion leads to reduced yield, which is detrimental to crop cultivation and ultimately food security. Though genetic studies have identified loci that affect the level of pollen heatwave tolerance in a few species, no causal genes have been identified, yet. Exploring natural variation for pollen heatwave tolerance is key to finding novel genetic elements involved in protection against damage. In this study, we developed a novel pollen phenotyping protocol, combining MTT-staining with automated image analysis for machine-learning-based pollen classification in Arabidopsis. This assay was employed to screen an Arabidopsis diversity panel consisting of 208 accessions originating from the Iberian Peninsula and Morocco exposed to a controlled long-term, heatwave-like temperature regime. Using GWAS, we identified a QTL encompassing a cluster of immune-associated nucleotide-binding protein (IAN) genes (*IAN2* to *IAN5*). The *ian2 ian3 ian4 ian5* quadruple mutant was more tolerant to heatwave-like conditions, indicating that these genes repress pollen viability under these conditions. These findings validate our novel phenotyping assay and, together with previous reports that IAN genes repress pollen tolerance to more severe heat, identify the IAN genes as candidate breeding targets for adaptation of crops to a warmer climate.

Keywords

Arabidopsis thaliana, pollen thermotolerance, heatwave, genome-wide association study (GWAS), image analysis, IAN genes

Introduction

As the global climate changes at a rapid pace, the intensity and frequency of extreme weather events such as heatwaves, i.e. elevated temperature spanning multiple days, increases (Meehl and Tebaldi 2004; Rahmstorf and Coumou 2011). Such conditions, while often stimulating vegetative growth, can have detrimental effects on sexual reproduction of plants.. While many genes have been related to the heat response (Chaturvedi et al. 2021; Huang et al. 2022), these findings were mostly done in the context of heat shock treatment, a sudden and short period of high temperature. Indeed, it has become increasingly clear that heat shock and heatwave-like conditions trigger distinctly different molecular pathways (Jansma et al. 2022). Mitigation of the detrimental effects of heatwave events on plant reproduction requires better understanding of the underlying genetic and physiological mechanisms.

Heat stress affects nearly all components of plant reproduction. However, as has been observed for a multitude of species, male reproductive development is especially sensitive to prolonged exposure to elevated temperatures (Wahid et al. 2007; Bita and Gerats 2013; Rieu et al. 2017). Successful pollen development is critical in the plant reproductive cycle and is highly sensitive to temperature increases, impacting seed quality and quantity (Müller and Rieu 2016). Reduction in fruit and/or seed set or yield under heatwave conditions was found to be strongly correlated to pollen viability in monocots, such as rice, sorghum, barley and wheat (Sakata et al. 2000; Peng et al. 2004; Prasad et al. 2006; Farooq et al. 2011; Wu et al. 2021), as well as dicots, such as tomato and cotton (Song et al. 2015; Xu et al. 2017; Driedonks et al. 2018). In Arabidopsis, there are some genes that have been linked to reproductive heat tolerance through reverse genetics. The unfolded protein response (UPR) signaling pathway and its RNA-splicing arm mediated through IRE1 was found to be important in maintaining male fertility under heat stress (Deng et al. 2016). The *ire1a ire1b* double mutant showed reduced pollen viability at elevated temperatures of 27.5°C during flowering (Deng et al. 2016). Additionally, ERdj3B, a gene involved in endoplasmic reticulum (ER) quality control, was found to play a role in anther development under heat stress (Yamamoto et al. 2020). KO-mutants grown at 29°C during reproductive stage showed reductions in seed set and pollen number and defects in pollen release (Yamamoto et al. 2020).

There have been some studies that attempted to unravel the genetics of pollen heatwave tolerance. In rice, a quantitative trait locus (QTL) analysis in a recombinant inbred line (RIL) population originating from the cross between a heat-tolerant and heat-sensitive cultivated line found two QTLs that were highly associated with pollen fertility in 3 day field trials with average air temperatures between 30.49 – 32.32°C (Xiao et al. 2011). In tomato, QTL analysis of an F2 population originating from the cross between a heat-tolerant and heat-sensitive genotype yielded a genomic region highly associated with pollen viability after 3 weeks heat treatment of 31/25°C day/night (Xu et al. 2017). While natural variation in reproductive heat response has been described previously in Arabidopsis (Warner and Erwin 2005; Lu et al. 2021), no study has investigated this for pollen specifically. Genetic analysis of Arabidopsis accessions revealed candidate loci for silique length after heat shock treatment of 35°C for 1 day during flowering (Bac-Molenaar et al. 2015). However, the genetic determinants were not studied regarding their role in heat-induced pollen defects. Natural variation for pollen heat tolerance promises to represent a trove of untapped genetic resources for further mechanistic studies and causal genes might in some cases directly translate to targets for crop improvement. This could be especially true given that anther and pollen development are genetically highly conserved processes (Gómez et al. 2015).

In this study, we aimed to discover genetic elements associated with pollen tolerance to heatwaves. To explore the extent of natural variation for this trait in the model plant *Arabidopsis thaliana*, we developed a robust pollen phenotyping assay for this species, combining conditional staining and microscopy with machine-learning-based image analysis and object classification. This assay was then applied to a panel of genetically diverse accessions, grown under long-term heatwave-like conditions. A genome-wide association analysis (GWAS) was performed combining phenotype and publicly available genotype data of these accessions to identify genomic regions associated with pollen heat tolerance.

Material and methods

Plant material and growth conditions

For development of image analysis pipeline, wild-type Arabidopsis (Col-0) was used. In addition, an Arabidopsis diversity panel ("Iberian^{+}") was selected consisting of 208 accessions to investigate phenotypic variation, and perform genetic analysis. The materials included 195 accessions from the Iberian panel from Spain and Portugal (Méndez-Vigo et al. 2011; Arteaga et al. 2021) and 13 accessions from Morocco (Durvasula et al. 2017), all obtained from the Nottingham Arabidopsis Stock Centre (Table S1). Finally, to investigate IAN-function under heatwave-like conditions, quadruple loss-of-function *ian2 ian3 ian4 ian5* mutant was obtained from (Lu et al. 2021). Seeds were sown on commercial soil (Lentse Potgrond number 4, Horticoop B.V., Katwijk, The Netherlands), and kept in a cold room at 4°C in the dark for 3 days to stratify. Subsequently, plants were cultivated in a regulated climate chamber, at 22 °C, vapor pressure deficit (VPD) 1.3 kPa (50% relative humidity (RH)), under LED-light (Philips Green Power LED DR/B/FR 120, ~200 µmol $m^{-2}s^{-1}$ at plant height) with a photoperiod of 16h/8h day/night (control). From four-leaf stage, or maximum of 10 days old, plants were kept at 4°C under LED-light with a photoperiod of 8h/16h day/night to undergo vernalization. Vernalization period was adjusted per accession based on an initial experiment where flowering times were recorded after 49 days of vernalization, and defined as number of days from sowing to first observed flower buds in the rosette. Based on the flowering time, accessions were grouped into one of three vernalization periods (28, 35, or 49 days; Table S1). After vernalization, plants were moved back to control conditions to acclimate to the climate chamber for a minimum of one week. Subsequently, when flowering started, plants were grown at 31 °C and VPD 1.3 kPa (72% RH), under LED-light with a photoperiod of 16h/8h day/night ("long-term mild heat"; LTMH), until pollen collection for viability staining.

Pollen viability staining

From each plant, flowers of stage 13 – when anthesis occurs where the flower opens and anther dehiscence (pollen release) occurs (Smyth et al. 1990; Alvarez-Buylla et al. 2010), corresponding to mature pollen release – were collected on two measuring days 7-12 days after start of the LTMH treatment. Anthers were dissected under a binocular and free pollen was suspended in 2.2 µL 10% sucrose MTT-solution (tetrazolium salts; (Khatun and Flowers 1995)) on a microscope slide under a 6 mm cover slide. After 30 minutes incubation in the dark, high-resolution images were acquired using a brightfield microscope (Leica DM5) equipped with DMC4500 Digital Microscope Camera (Leica). Per sample, ~190 images were acquired at 20X magnification to encompass the entire cover slide. MTT treatment was expected to result in purple staining in viable pollen, and no staining in inviable pollen.

Automated image analysis

All images of a sample were merged and files were exported to TIFF-file format for downstream analysis using the Leica LASX software (Leica Microsystems). An automated image analysis pipeline was developed to obtain pollen viability phenotypes. The pipeline comprised three main parts: object segmentation, object measurement, and object classification (Fig. S1). Object segmentation was performed using the deep-learning-based segmentation method from *cellpose* (Stringer et al. 2021) with default model *cyto2* and object diameter set to 95 pixels, yielding outlines for all recognized objects (e.g. pollen) in the original TIFF-file saved in PNG-file format. Object measurement was performed using a Python-based distribution of *ImageJ2* (*pyimagej*) with *Fiji* plugins *MorphoLibJ* (Legland et al. 2016), and plugins from the BioImaging and Optics Platform (PTBIOP) Fiji update site (Schindelin et al. 2012). PNG-files were used to create regions-of-interest (ROIs) in the TIFF-file, and from the objects outlined by ROIs a subset of parameters was measured (Table S2). Object classification was performed using machine learning (ML) algorithms from the Python library *scikit-learn* (Kramer 2016).

Invoking *RandomForestClassifier(n_estimators=100)*, a model was trained using a dataset of 1799 manually classified MTT-stained pollen from images of different genotypes of *Arabidopsis thaliana*. With *ShuffleSplit(n_splits=10, test_size=0.2)*, training and test datasets were generated multiple times with a ratio of 4:1 (train/test), randomizing train and test dataset composition each time. Objects obtained from the images were classified as either 'aborted pollen', 'live pollen', or 'non-pollen'. The last class consisted mostly of tissue debris, dust specks, air bubbles and pixel artifacts. Additionally, based on a bimodal size distribution in the 'aborted pollen' class, pollen belonging to this class were further divided into two subclasses: 'early aborted pollen' or 'late aborted pollen'. Model

performance was evaluated by averaging accuracy across the ShuffleSplit iterations. After performance evaluation, the classifier was retrained on the full manually classified pollen dataset to maximize the amount of training data available for the final model.

Climate and geographical data

Climate index datasets were downloaded from E-OBS (Cornes et al. 2018). The ensemble mean datasets from E-OBSv29.0e and its derivative indices were used for correlation analysis with physiological traits of accessions. E-OBS ensemble means were estimated on a grid with resolution of 0.1°. For each accession, climate variable estimates were assigned corresponding to the grid square nearest to their actual coordinates of collection.

Statistical analysis of phenotype data

All statistical analyses were performed using R 4.3.2 (R Core Team 2025). From the object classification, three derived pollen phenotypes were determined: pollen viability (PV), early heat tolerance (EHT), and late heat tolerance (LHT). These were calculated as follows:

$$PV = 100 * \frac{\#\ live\ pollen}{\#\ total\ pollen}$$

$$EHT = 100 * \frac{\#\ live\ pollen\ +\ \#\ late\ aborted\ pollen}{\#\ total\ pollen}$$

$$LHT = 100 * \frac{\#\ live\ pollen}{\#\ live\ pollen +\ \#\ late\ aborted\ pollen}$$

For statistical analyses, PV, EHT, and LHT data were logit-transformed using the *car* package (Fox 2007), according to:

$$value' = \log[\frac{value/100}{1 - value/100}]$$

Correlation analyses were done using Pearson's correlation test.

Genome-wide association mapping

Genome-wide association study (GWAS) was performed with Efficient Mixed-Model Association eXpedited (EMMAX) software (Kang et al. 2010), using the mean phenotype values for 1-4 replicates of each accession. The Iberian SNP dataset was described previously (Tabas-Madrid et al. 2018; Arteaga et al. 2021). In brief, this dataset consisted of 2,186,721 SNPs for the 232 Iberian accessions in this study, for which MAF > 3 and Missingness < 45%. This was combined with SNP data for the 18 Moroccan accessions (Durvasula et al. 2017) based on their alignment to the TAIR10 reference genome and only SNPs were kept which were present in all accessions, resulting in a final dataset of 1,761,625 SNPs. Ultimately, analysis was done with 208 out of 254 accessions for which phenotypic data was available. Effects of genotype and environmental variables were tested by the following model:

$$Y_i = \mu + G_i + E_i + e_i$$

Where Y_i is the phenotypic value of genotype i, μ the overall mean, G_i the fixed effect of genotype i, E_i the fixed effects of environmental variables, including sampler, growth chamber location, and technical replicate, and e_i the residual error effect. Phenotypic values were corrected according to the fixed effect of genotype, prior to association

mapping. The Balding-Nichols kinship matrix was calculated using the default command and was included as covariate to correct for population structure, by default (Fig. S3). Additionally, narrow-sense heritability for each trait was calculated by EMMAX from the genetic relatedness described by the kinship matrix. For association, a stringent threshold was applied of -log10(0.05/1,761,625) = 7.55, corresponding to 5% with Bonferroni correction for multiple testing. Additionally, a lower threshold of -log10(1/1,761,625) = 6.25 was applied to obtain potential associations (Jiang et al. 2020). Manhattan plots of association results and corresponding Q-Q plots were generated using the *qqman* and *ggplot2* packages (Turner 2014) in R 4.3.2 (R Core Team 2025).

Results

Image-based classification of pollen in an Arabidopsis diversity panel exposed to heatwave-like conditions

Using MTT staining and manual evaluation, we found that cultivation of Arabidopsis accession Col-0 at 31 °C significantly reduced the viability of mature pollen when plants were exposed for a period of at least 7 days (Fig. 1). To study the genetic basis of tolerance of pollen development to such heatwave-like long-term mild heat (LTMH) conditions, an "Iberian+" diversity panel was composed by expanding the Iberian diversity panel (Arteaga et al. 2021) with accessions from Morocco (Durvasula et al. 2017) to a total of 208 accessions (Table S1) and plants were exposed to long-term mild heat (LTMH) for 7-12 days during the flowering stage. Pollen were stained for viability and imaged, after which pollen-like objects were identified from the images using a deep-learning-based segmentation approach. 1799 objects originating from 15 randomly selected accessions were classified manually and used as a train/test set to develop a random-forest classification model. Objects were first classified as being pollen or non-pollen. From the acquired pollen staining images of the diversity panel, we observed a bimodal size distribution within the aborted pollen class (Fig. S2). Thresholds were set on area values to separate aborted pollen into two subclasses: early aborted pollen (small area value) or late aborted pollen (large area value). We maintained three different threshold area values to define early and late aborted pollen. The objects in the train/test dataset were classified based on these thresholds. We selected a random forest model trained on a lenient pixel value threshold and an area threshold with a low ratio early to late aborted pollen.

The random forest model was trained on the measurement variables of the train/test dataset. First, the train/test dataset was shuffled and split ten-fold at a 4:1 (train:test) ratio. It achieved an overall accuracy of 0.898% across cross-validation folds (Table 1). For each class, we calculated precision (e.g. ratio at which the model correctly predicts class), recall (e.g. ratio of real samples the model actually found) and F1-score (e.g. average between precision and recall).

Table 1 Classification performance of random forest model

	Precision	**Recall**	**F1-score**	**Support**
Aborted	0.831	0.825	0.828	859
Alive	0.922	0.940	0.931	2130
Other	0.910	0.856	0.882	611
Accuracy			**0.898**	3600
Macro average	0.887	0.874	0.880	
Weighted average	0.898	0.898	0.898	

Class-wise performance varied, with highest performance observed for class 'Alive' (F1-score = 0.931), followed by class 'Other' (F1-score = 0.882), and class 'Aborted' (F1-score = 0.828; Table 1). The lower performance of class 'Aborted' indicated that a proportion of this class was misclassified (Table 1). The aggregated confusion matrix, which

sums up the predictions of the ten-fold cross-validation revealed that misclassified class 'Aborted' samples were primarily assigned to class 'Alive' (Fig. 2). The model exhibited a reduced sensitivity for the class 'Aborted', but otherwise performed robustly. This random forest model was then used to predict pollen classes from the images of stained collected for the diversity panel.

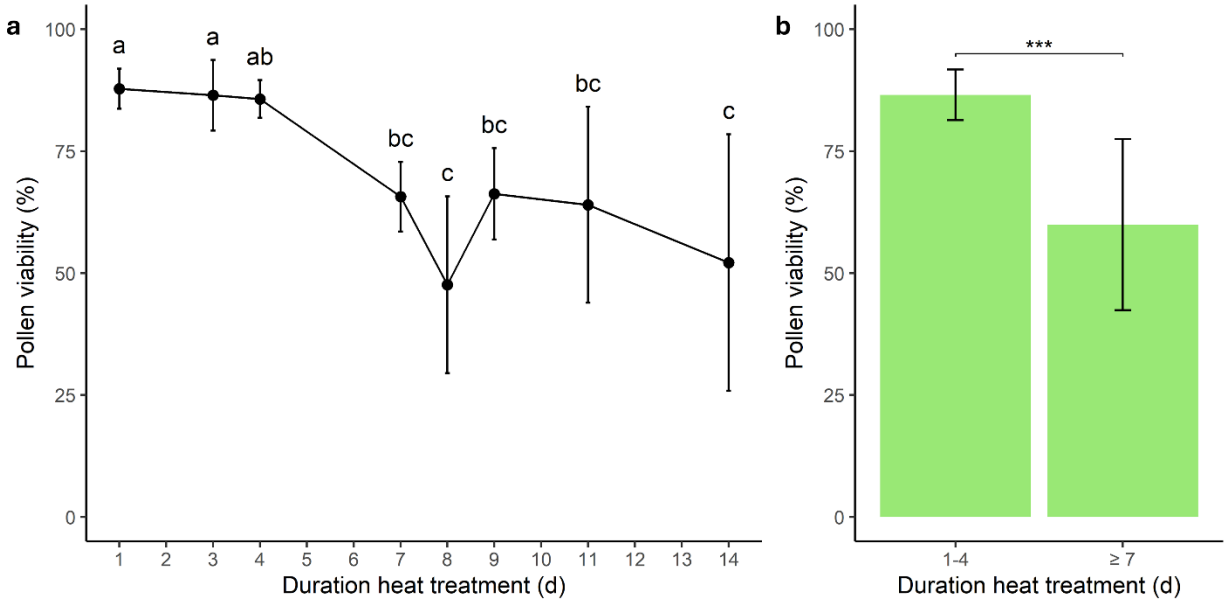

Fig. 1 Effect of long-term mild heat (LTMH) on viability of mature pollen. a. Flowering Arabidopsis plants (accession Col-0) were exposed to 31 °C and mature pollen were sampled from freshly opened flowers at various days after the start of treatment. Shown is mean pollen viability, with error bars denoting standard deviation (n=8). Different letters show significant difference as determined by one-way ANOVA and post-hoc Tukey's test using logit-transformed pollen viability values ($p \leq 0.05$). b. Comparison of short-term versus long-term mild heat treatment. Shown is mean pollen viability, with error bars denoting standard deviation, grouping 1-4 days and ≥7 days of treatment (n=24 and 32, respectively). Asterisks indicate significant difference as determined by Student's T-test (*, $p \leq 0.05$; **, $p \leq 0.01$, ***, $p \leq 0.001$)

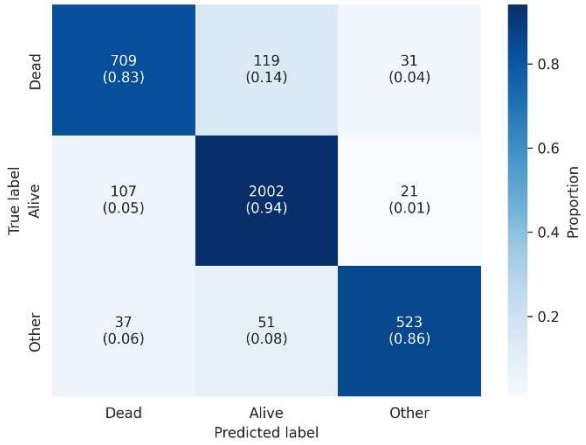

Fig. 2 Heat map of aggregated cross-validation results of random forest model. Shown is, for each class ('Aborted', 'Alive', 'Other'), the sum of all objects across ten folds of cross-validation and the normalized recall (proportion) between brackets. The values on the top-left to lower-right diagonal panes show objects correctly predicted by the model

The Iberian^{+} diversity panel captures wide phenotypic variation for pollen viability under heatwave-like conditions

The pollen classification data from the automated image-analysis pipeline was used to determine overall pollen viability (PV) upon exposure to LTMH for each accession of the diversity panel, as well as the early heat tolerance (EHT), late heat tolerance (LHT) (Table S1), revealing considerable natural variation for these traits (Fig. 3). While LHT correlated positively with PV over the whole PV range, low EHT was strongly biased towards the ~25% of accessions with lowest PV (Fig. 3c-f).

The geographical origin of the accessions ranged from latitudes of 31.24986 to 43.54986 degrees, longitudes of -8.65014 to 2.64986 degrees and elevations of 12 to 2388 meters above sea level (Fig. 3b; Table S1). To determine whether adaptation to local conditions had occurred within the population, we performed a correlation analysis between pollen viability data and a multitude of geographical and climatic variables. Based on Pearson's correlation coefficients, we observed no significant correlation between PV and any of these variables (Table S3).

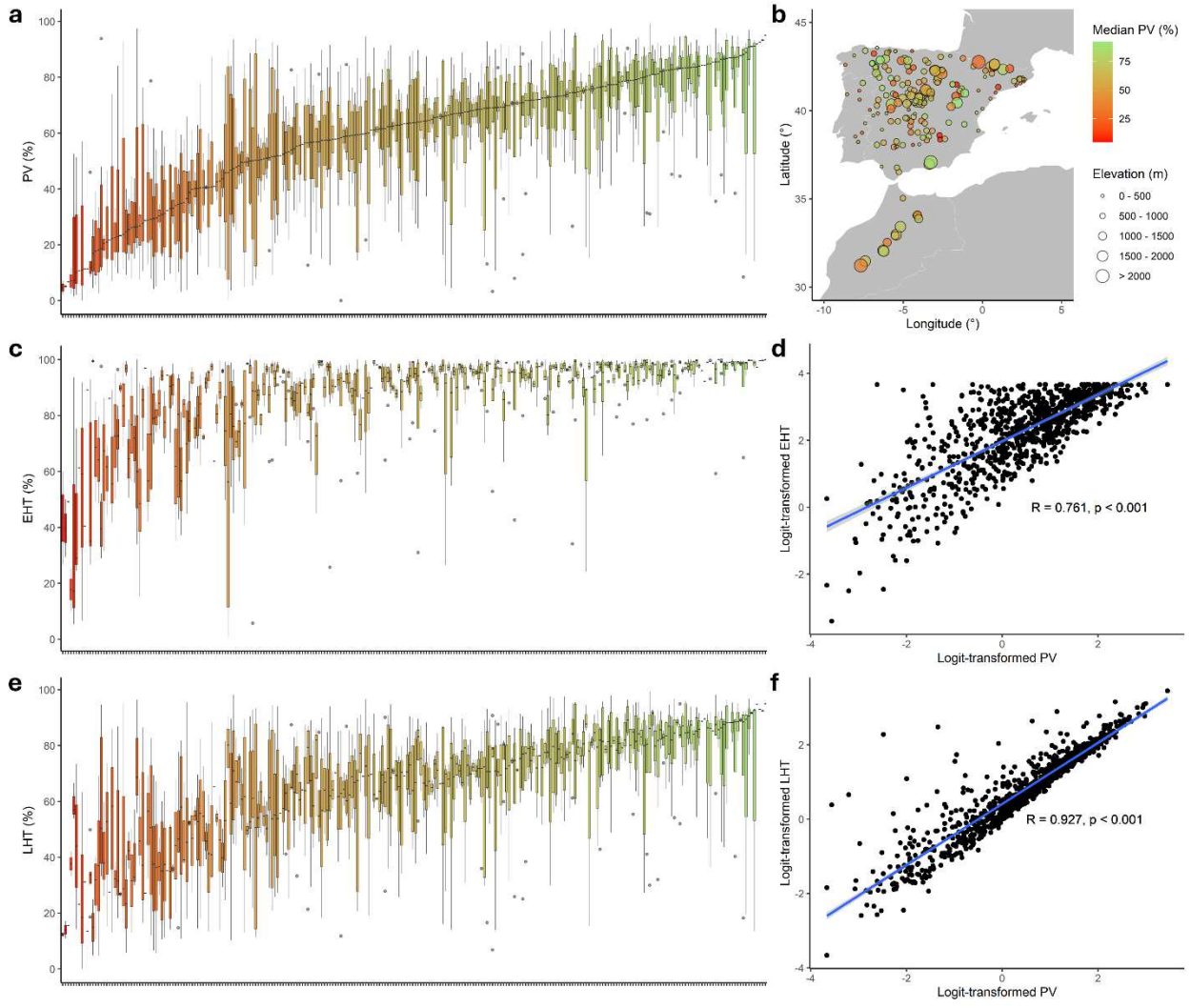

Fig. 3 Phenotypic variation in pollen traits after LTMH treatment among accessions of the Iberian^{+} diversity panel. a. Pollen viability (PV) of each accession under LTMH conditions, ranked low to high based on mean value. b. Geographic distribution of natural accessions from the Iberian^{+}

diversity panel. c and e. EHT (EHT; c) and LHT (LHT; e) under LTMH, with accessions on the y-axis ordered as in a. Pearson correlation between logit-transformed PV and logit-transformed EHT (d) and LHT (f). Colors in panes a, b, c and e reflect median PV(%) for each accession according to the scale shown in b

GWAS reveals QTL for pollen viability under heatwave-like conditions

To identify genetic determinants of pollen heat tolerance, GWAS was performed. To test the functionality of our panel and GWAS pipeline, we first analyzed the trait flowering time, which was scored during plant cultivation. A single major QTL was found, centered on the known flowering time gene TWIN SISTER OF FT (TSF; Yamaguchi et al. 2005), thus validating the applied methods (Fig. S4).

For overall pollen viability, we found a single peak on chromosome 1 that was significantly associated with the trait, which we called qPV1 (Fig. 4a; Table 2). The QTL was supported by a trailing string of SNPs in which the peak position is centred. As could be observed from Q-Q plots of the expected versus observed association values, there was no indication of genome-wide inflation, suggesting an absence of systematic bias (e.g., due to population structure or relatedness), which further validates peak significance (Fig. 4b). Narrow-sense heritability (h^2) for the pollen viability trait was ~10%, as calculated by EMMAX, based on the genetic relatedness from the kinship matrix.

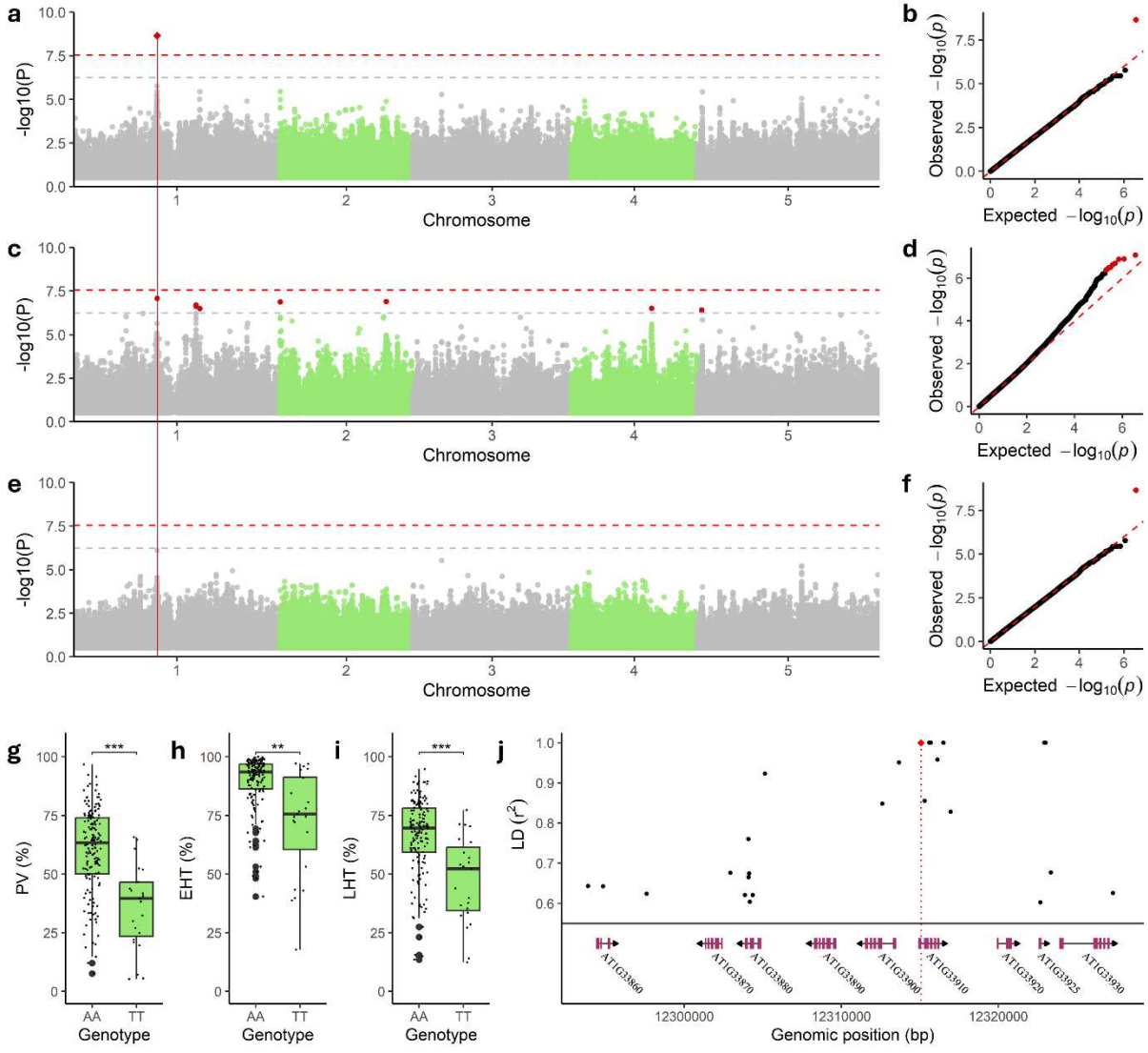

Fig. 4 GWAS results for pollen traits under LTMH treatment for accessions of the Iberian$^+$ diversity panel. a, c, e. Manhattan plot showing GWAS results for PV (a), EHT (c) and LHT (e). Stringent and more lenient significance thresholds are indicated as dashed red and grey lines, respectively. Vertical red lines indicate position of qPV1. b, d, f. Q-Q plot for GWAS results for PV (b), EHT (d) and LHT (f). g-i. PV (g), EHT (h) and LHT (i) of Iberian$^+$ accessions, grouped by allele at qPV1. Asterisks denote significance as determined by Student's T-test (**, p≤0.01; ***, p≤0.001). j. Linkage disequilibrium (LD) between qPV1 (red diamond) and neighboring SNPs (black dots). Genomic positions of genetic elements in the candidate region is indicated at the bottom

Table 2 Association results for QTLs for pollen viability (PV), early heat tolerance (EHT), and late heat tolerance (LHT)

QTL	SNP	CHR	BP	LOD*
qPV1	1_12315077	1	12,315,077	8.7
qEHT1-1	1_12315077	1	12,315,077	7.1
qEHT1-2	1_18054124	1	18,054,124	6.6
qEHT1-3	1_18056662	1	18,056,662	6.7
qEHT1-4	1_18650079	1	18,650,079	6.5
qEHT2-1	2_109941	2	109,941	6.9
qEHT2-2	2_15769226	2	15,769,226	6.9
qEHT4	4_11876908	4	11,876,908	6.5
qEHT5-1	5_707566	5	707,566	6.4
qEHT5-2	5_708303	5	708,303	6.4

CHR, chromosome; BP, base pair position.
*, shown is the -log10(p)-value for the most associated SNPs.

Seven significant SNP associations were found for EHT (Fig. 4c; Table 1). Notably, the most significant qEHT1-1 corresponded to qPV1 and several of the other QTLs, i.e. qEHT1-3, 2-1 and 5-1, showed a corresponding non-significant peak for PV. No significant SNP associations were identified for LHT, but the highest association again corresponded to qPV1 and a clear non-significant peak with trail on chromosome 5 was also mirrored in the PV plot (Fig. 4e).

qPV1 existed as two alleles in the panel, with the peak SNP being A or T. Accessions homozygous for allele A had significantly higher PV and both, higher EHT and higher LHT than accessions homozygous for allele T (Fig. 4g-i). We determined the QTL interval on chromosome 1 through LD analysis of the peak SNP and neighboring SNPs (Fig. 4j) and found the peak SNP to be located in exon 1 of *immune-associated nucleotide-binding 5* (*IAN5*; AT1G33910). Additionally, neighboring SNPs in strong linkage with the peak SNP ($r^2 > 0.9$) localized to a region containing six genes, spanning from *IAN2* (AT1G33880) to a small protein-coding gene (AT1G33925). The other four genes in this interval were IAN paralogs, namely *IAN3* (AT1G33890), *IAN4* (AT1G33900), *IAN5* (AT1G33910) and Phloem Protein 2-A4 (AT1G33920).

qPV1 shows interaction with other potential QTL

To investigate whether PV was determined by a single locus in our study or by the combined action of multiple QTLs, we compared individuals harboring either the tolerant or sensitive allele of qPV1 in combination with the tolerant or sensitive alleles of any of the other EHT QTLs. Individuals harboring the tolerant allele for qPV1, already had significantly lower PV if they also harbor the sensitive allele for qEHT1-2 (GG), qEHT2-1 (TT), qEHT2-2 (TT), and qEHT4 (TT; Fig. 5a/c/d/e). Furthermore, no significant interactive effects were found between these QTLs and qPV1. The same observation could be made for qEHT1-3, but due to the small group sizes, these results may be slightly skewed (Fig. 5b). Interestingly, for qEHT5-1 a significant interaction is observed, whereby individuals harboring the sensitive allele for both QTLs have a significantly lower PV than those harboring only the sensitive allele for qPV1 (Fig. 5f).

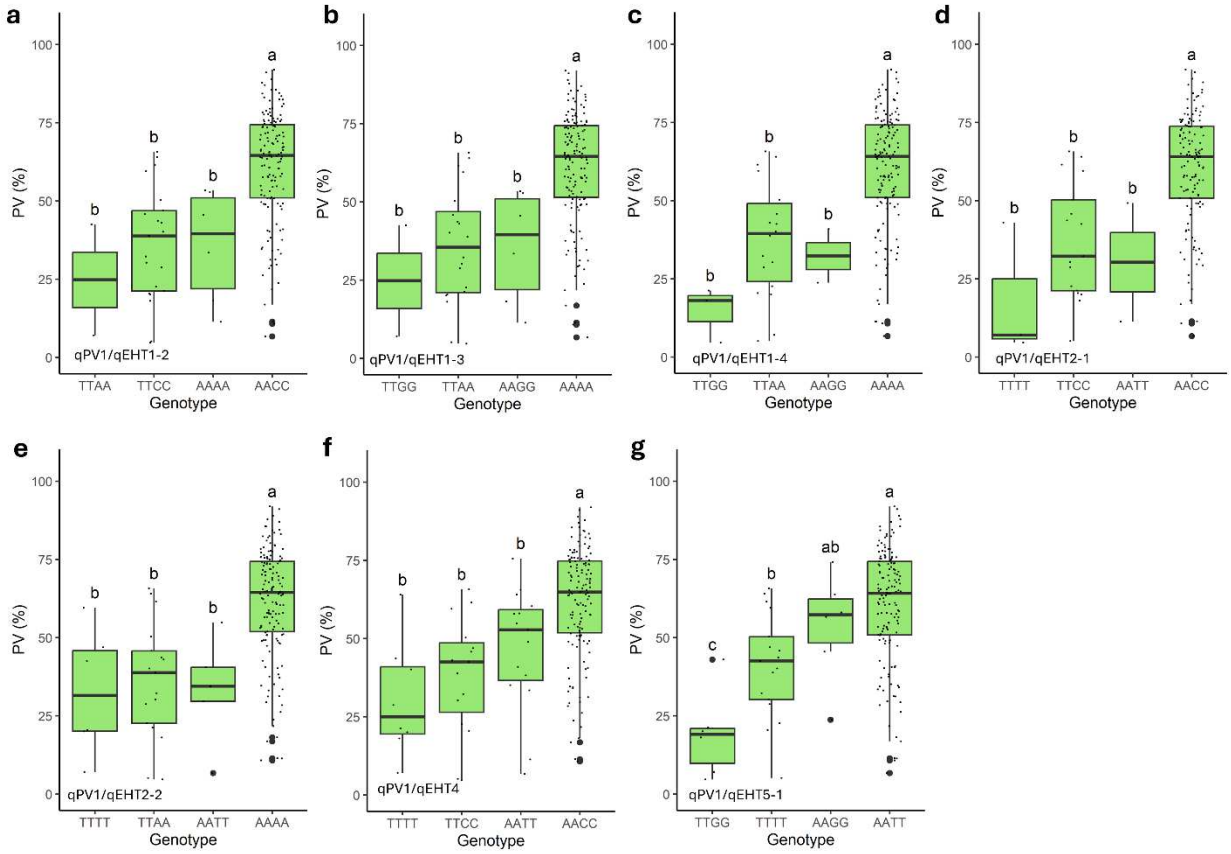

Fig. 5 Interaction between qPV1 and other potential QTLs. Shown is PV (%) for Iberian^{+} accessions grouped by genotype for qPV1 and qEHT1-2 (a), qEHT1-3 (b), qEHT2-1 (c), qEHT2-2 (d), qEHT4 (e), and qEHT5-1 (f), respectively. First and second letter for genotype indicate genotype for qPV1, third and fourth letter indicate genotype for the second QTL. Different letters above boxplots show significant difference as determined by one-way ANOVA and post-hoc Tukey's test using logit-transformed PV values ($p<0.05$). Bold dots indicate outliers per group.

Knockout of IAN genes leads to higher pollen viability under heat

To confirm the role of the IAN gene cluster in heat-induced pollen abortion, we compared pollen viability of a quadruple loss-of-function *ian2 ian3 ian4 ian5* mutant (Lu et al. 2021) and the corresponding wild type (Col-0) under heatwave-like conditions (Fig. 6) and found that it was significantly higher in KO-mutants.

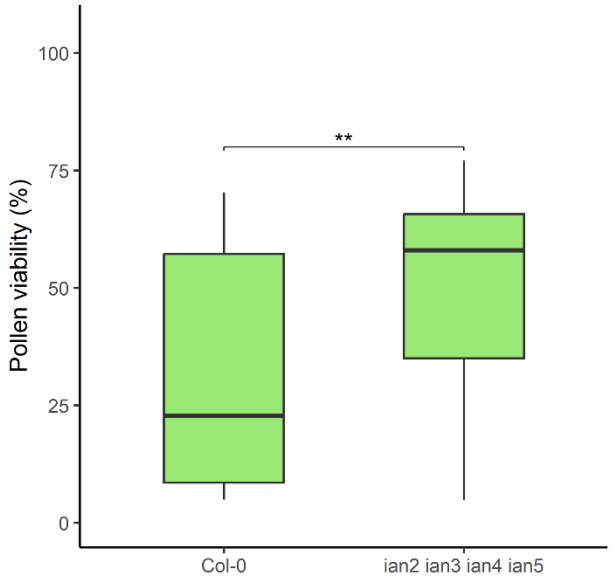

Fig. 6 Quadruple IAN gene KO-mutant. Shown is pollen viability for wild type (Col-0; n=31) and quadruple *ian2 ian3 ian4 ian5* KO-mutant (n=27). Asterisks denote significance as determined by Student's T-test (**, p≤0.01)

Discussion

Given the need for crops varieties with better male heatwave tolerance, in this study, we developed a pollen viability analysis pipeline for the model plant Arabidopsis and explored the natural variation in pollen tolerance to heatwaves in a diversity panel to discover genetic elements associated with the trait.

Novel image analysis-based pollen phenotyping protocol for Arabidopsis

GWAS requires consistent and standardized protocols to phenotype a large numbers of individuals. In this study, we successfully developed a novel "medium throughput" protocol, which combines pollen staining with machine learning (ML)-based image analysis to automatically classify pollen. Automated pollen viability classification has already been applied in a variety of species, including Arabidopsis, rice (Castle-Green et al.), and tomato (Phumeechanya et al. 2024). Both studies used a deep neural network approach. Also, similar learning tools have been used in the classification of pollen to species level for palynological analyses (Sevillano and Aznarte 2018; Dunker et al. 2021; Olsson et al. 2021; Barnes et al. 2023; Gallardo et al. 2024). With any automatic classification approach trade-offs often must be made between hardware/development costs, processing time, and model accuracy. The model we developed vastly improved on processing time of pollen samples as opposed to manual counting and provided high accuracy, making it suitable for large-scale evaluations.

Extreme variation for pollen viability and its subtraits under heatwave conditions in the Iberian^{+} diversity panel

To investigate phenotypic variation in Arabidopsis pollen thermotolerance we applied our phenotyping protocol to phenotype a diversity panel of 208 accessions (Iberian^{+} panel). Large variation in pollen heatwave tolerance was observed in this panel, with pollen viability (PV) ranging from 5% to 95%. Phenotypic variation in the context of abiotic stress in natural populations is often attributed to local adaptation. For example, Arabidopsis seedling survival and root growth responses under heat stress have been found to be correlated to local climate components (Zhang et

al. 2015). Also, reproductive traits in wild relatives of tomato subjected to long-term mild heat were weakly but significantly correlated to the mean annual temperature at their geographic origins (Driedonks et al. 2018).

However, our study did not find evidence for local adaptation for the Iberian^{+} diversity panel. A possible explanation might be that pollen heat tolerance is shaped, directly or indirectly, by other evolutionary constraints, such as trade-offs with other (a)biotic stress tolerance traits.

Overall pollen survival seems to be dictated by the interplay between EHT and LHT

Heat stress significantly affects pollen development by causing pollen abortion and reducing pollen viability. Pollen viability in Arabidopsis was found to be affected by heatwave conditions at a minimal duration of eight days. Eight days before anthesis, flower buds are at stage 7-8, which marks the moment of microspore release from the tetrads, prior to tapetal degeneration (Sanders et al. 1999; Wiese et al. 2024). We observed a bimodal distribution in sizes in aborted pollen, suggesting that there are two moments of abortion, i.e. one during microspore development and one during late pollen development. The chance of a developing pollen surviving the late abortion moment (LHT) was very strongly related to overall PV over the whole range of PVs. The chance of a pollen surviving the early abortion moment (EHT) was not independent of LHT, as it only dropped in accessions where LHT was below ~50%, which comprised ~25% of the population. One explanation could be that the high temperature damage occurs during early microspore development, as described for many species (De Storme and Geelen 2014) and that in the most sensitive accessions pollen abort immediately, while in the more tolerant accessions this happens at a later stage, or not at all. Indeed, in tomato, early heat exposure led to abortion after mitosis (Xu et al. 2022). Thus, EHT and LHT may represent the same trait. This agrees with the fact that the strongest genetic associations for EHT, LHT and PV were found at the same locus. Previously, it was found that 48h exposure at 30-32°C caused meiotic defects in developing microspores in flowering Arabidopsis, leading to dyad and even polyad formation (De Storme and Geelen 2020). However, microspores with aberrant meiotic events did not arrest and all developed into mature pollen after heat treatment (De Storme and Geelen 2020). The occurrence of such aberrant pollen of larger size was not recorded in this study.

GWAS reveals an IAN gene cluster associated with pollen thermotolerance

Narrow-sense heritability (h^2), the proportion of the phenotype explained by genome-wide relatedness, in this panel was considered quite low for pollen thermotolerance (~10%). Low heritability would point to strong environmental influences or a polygenic trait architecture. Indeed, the large variation between replicate observations per line would confirm the former. It is also well conceivable that pollen viability at high temperature is a polygenic trait, as it would be dependent on many developmental and physiological processes taking place in a short timeframe (Rieu et al. 2017). However, there was no genome-wide inflation of associated SNPs in our Q-Q plot for PV, and only one SNP was statistically significant in the GWAS for PV and had a considerable effect size (e.g. ~25% PV).

This SNP is located within the coding sequence of *immune-associated nucleotide-binding 5* (*IAN5*), a member of a cluster of IAN genes (IAN2-6) on chromosome 1 that were previously shown to inhibit the unfolded protein response and promote cell death in response to heat stress (Lu et al. 2021). LD analysis revealed the qPV1 locus to span the genomic region containing *IAN2* through *IAN5*, highlighting all these genes as candidate modulators of pollen viability. This was supported by the increased pollen heat tolerance in the quadruple *ian2 ian3 ian4 ian5* knockout grown in our long-term mild heat conditions. This result indicates that these IAN genes repress heat tolerance in pollen. Previously, a GWAS found the same IAN gene cluster to be associated with flower fertility following a shorter and more severe heat treatment of 35 °C for 40 h during early flower development. In that study, IAN loss-of-function mutants showed improved fertility upon exposure to this heat profile (Lu et al. 2021). Moreover, developing pollen from both, the *ian2 ian3 ian4 ian5* and the *ian6* single mutants had higher heat tolerance than the wild type, and pollen from a rice *ian1* knockout mutant were found to be more tolerant to exposure of plants to 48 °C for 3 hours. Thus, our study confirmed the involvement of IAN genes in determining heat tolerance level and found that this applies not only to short exposure to severe heat, but also to long-term exposure to milder high temperatures.

Taken together, we identified a novel genetic determinant of pollen heatwave tolerance. Future studies should reveal whether this can be translated to crop species.

Availability of materials

Data supporting the findings of this study are available within the paper and its Supplementary Information, and in the Zenodo repository at https://doi.org/10.5281/zenodo.23033916.

Statements and Declarations

Competing interests

Funding Declaration

This work was funded by the Dutch Research Council (NWO; grant number 18039, to Ivo Rieu).

Author contributions

The study was designed by IR and MF. Screening of the Iberian^{+} diversity panel was executed by JH and MF. Automatic image analysis and pollen classification scripts were designed by DB and MF. Mutant analysis was performed by LK. Statistical analysis of data was done by MF and ES. The article was written by MF with commentary provided by ES and IR.

References

Alvarez-Buylla ER, Benítez M, Corvera-Poiré A, Chaos Cador Á, de Folter S, Gamboa de Buen A, Garay-Arroyo A, García-Ponce B, Jaimes-Miranda F, Pérez-Ruiz RV, Piñeyro-Nelson A, Sánchez-Corrales YE (2010) Flower Development. Arab Book Am Soc Plant Biol 8:e0127. https://doi.org/10.1199/tab.0127

Arteaga N, Savic M, Méndez-Vigo B, Fuster-Pons A, Torres-Pérez R, Oliveros JC, Picó FX, Alonso-Blanco C (2021) MYB transcription factors drive evolutionary innovations in Arabidopsis fruit trichome patterning. Plant Cell 33(3):548–565. https://doi.org/10.1093/plcell/koaa041

Bac-Molenaar JA, Fradin EF, Becker FFM, Rienstra JA, van der Schoot J, Vreugdenhil D, Keurentjes JJB (2015) Genome-Wide Association Mapping of Fertility Reduction upon Heat Stress Reveals Developmental Stage-Specific QTLs in Arabidopsis thaliana. Plant Cell 27(7):1857–1874. https://doi.org/10.1105/tpc.15.00248

Barnes CM, Power AL, Barber DG, Tennant RK, Jones RT, Lee GR, Hatton J, Elliott A, Zaragoza-Castells J, Haley SM, Summers HD, Doan M, Carpenter AE, Rees P, Love J (2023) Deductive automated pollen classification in environmental samples via exploratory deep learning and imaging flow cytometry. New Phytol 240(3):1305–1326. https://doi.org/10.1111/nph.19186

Bita C, Gerats T (2013) Plant tolerance to high temperature in a changing environment: scientific fundamentals and production of heat stress-tolerant crops. Front Plant Sci 4. https://doi.org/10.3389/fpls.2013.00273

Castle-Green S, Pound MP, Pridmore TP Counting Pollen Viability via Deep Learning

Chaturvedi P, Wiese AJ, Ghatak A, Záveská Drábková L, Weckwerth W, Honys D (2021) Heat stress response mechanisms in pollen development. New Phytol 231(2):571–585. https://doi.org/10.1111/nph.17380

Cornes RC, van der Schrier G, van den Besselaar EJM, Jones PD (2018) An Ensemble Version of the E-OBS Temperature and Precipitation Data Sets. J Geophys Res Atmos 123(17):9391–9409. https://doi.org/10.1029/2017JD028200

De Storme N, Geelen D (2014) The impact of environmental stress on male reproductive development in plants: biological processes and molecular mechanisms. Plant Cell Environ 37(1):1–18. https://doi.org/10.1111/pce.12142

De Storme N, Geelen D (2020) High temperatures alter cross-over distribution and induce male meiotic restitution in Arabidopsis thaliana. Commun Biol 3(1):187. https://doi.org/10.1038/s42003-020-0897-1

Deng Y, Srivastava R, Quilichini TD, Dong H, Bao Y, Horner HT, Howell SH (2016) IRE1, a component of the unfolded protein response signaling pathway, protects pollen development in Arabidopsis from heat stress. Plant J 88(2):193–204. https://doi.org/10.1111/tpj.13239

Driedonks N, Wolters-Arts M, Huber H, de Boer G-J, Vriezen W, Mariani C, Rieu I (2018) Exploring the natural variation for reproductive thermotolerance in wild tomato species. Euphytica 214(4):67. https://doi.org/10.1007/s10681-018-2150-2

Dunker S, Motivans E, Rakosy D, Boho D, Mäder P, Hornick T, Knight TM (2021) Pollen analysis using multispectral imaging flow cytometry and deep learning. New Phytol 229(1):593–606. https://doi.org/10.1111/nph.16882

Durvasula A, Fulgione A, Gutaker RM, Alacakaptan SI, Flood PJ, Neto C, Tsuchimatsu T, Burbano HA, Picó FX, Alonso-Blanco C, Hancock AM (2017) African genomes illuminate the early history and transition to selfing in Arabidopsis thaliana. Proc Natl Acad Sci 114(20):5213–5218. https://doi.org/10.1073/pnas.1616736114

Farooq M, Bramley H, Palta JA, Siddique KHM (2011) Heat Stress in Wheat during Reproductive and Grain-Filling Phases. Crit Rev Plant Sci 30(6):491–507. https://doi.org/10.1080/07352689.2011.615687

Fox J (2007) The car Package

Gallardo R, García-Orellana CJ, González-Velasco HM, García-Manso A, Tormo-Molina R, Macías-Macías M, Abengózar E (2024) Automated multifocus pollen detection using deep learning. Multimed Tools Appl 83(28):72097–72112. https://doi.org/10.1007/s11042-024-18450-2

Gómez JF, Talle B, Wilson ZA (2015) Anther and pollen development: A conserved developmental pathway. J Integr Plant Biol 57(11):876–891. https://doi.org/10.1111/jipb.12425

Huang L-Z, Zhou M, Ding Y-F, Zhu C (2022) Gene Networks Involved in Plant Heat Stress Response and Tolerance. Int J Mol Sci 23(19):11970. https://doi.org/10.3390/ijms231911970

Jansma SY, Sergeeva LI, Tikunov YM, Kohlen W, Ligterink W, Rieu I (2022) Low Salicylic Acid Level Improves Pollen Development Under Long-Term Mild Heat Conditions in Tomato. Front Plant Sci 13. https://doi.org/10.3389/fpls.2022.828743

Jiang H-L, Hong J, Jiang Y-T, Yu S-X, Zhang Y-J, Shi J-X, Lin W-H (2020) Genome-Wide Association Analysis Identifies Candidate Genes Regulating Seed Number per Silique in Arabidopsis thaliana. Plants 9(5):585. https://doi.org/10.3390/plants9050585

Kang HM, Sul JH, Service SK, Zaitlen NA, Kong S, Freimer NB, Sabatti C, Eskin E (2010) Variance component model to account for sample structure in genome-wide association studies. Nat Genet 42(4):348–354. https://doi.org/10.1038/ng.548

Khatun S, Flowers TJ (1995) The estimation of pollen viability in rice. J Exp Bot 46(1):151–154. https://doi.org/10.1093/jxb/46.1.151

Kramer O (2016) Scikit-Learn. In: Kramer O (ed) Machine Learning for Evolution Strategies. Springer International Publishing, Cham, pp 45–53

Legland D, Arganda-Carreras I, Andrey P (2016) MorphoLibJ: integrated library and plugins for mathematical morphology with ImageJ. Bioinformatics 32(22):3532–3534. https://doi.org/10.1093/bioinformatics/btw413

Lu S, Zhu T, Wang Z, Luo L, Wang S, Lu M, Cui Y, Zou B, Hua J (2021) *Arabidopsis immune-associated nucleotide-binding* genes repress heat tolerance at the reproductive stage by inhibiting the unfolded protein response and promoting cell death. Mol Plant 14(2):267–284. https://doi.org/10.1016/j.molp.2020.11.010

Meehl GA, Tebaldi C (2004) More Intense, More Frequent, and Longer Lasting Heat Waves in the 21st Century. Science 305(5686):994–997. https://doi.org/10.1126/science.1098704

Méndez-Vigo B, Picó FX, Ramiro M, Martínez-Zapater JM, Alonso-Blanco C (2011) Altitudinal and Climatic Adaptation Is Mediated by Flowering Traits and FRI, FLC, and PHYC Genes in Arabidopsis. Plant Physiol 157(4):1942–1955. https://doi.org/10.1104/pp.111.183426

Olsson O, Karlsson M, Persson AS, Smith HG, Varadarajan V, Yourstone J, Stjernman M (2021) Efficient, automated and robust pollen analysis using deep learning. Methods Ecol Evol 12(5):850–862. https://doi.org/10.1111/2041-210X.13575

Peng S, Huang J, Sheehy JE, Laza RC, Visperas RM, Zhong X, Centeno GS, Khush GS, Cassman KG (2004) Rice yields decline with higher night temperature from global warming. Proc Natl Acad Sci 101(27):9971–9975. https://doi.org/10.1073/pnas.0403720101

Phumeechanya S, Chatchawankanphanich O, Duangjit J (2024) Pollenquanttom: A Novel Deep Learning Tool for Discriminating Viable and Non-Viable Tomato Pollen

Prasad PVV, Boote KJ, Allen LH (2006) Adverse high temperature effects on pollen viability, seed-set, seed yield and harvest index of grain-sorghum [*Sorghum bicolor* (L.) Moench] are more severe at elevated carbon dioxide due to higher tissue temperatures. Agric For Meteorol 139(3):237–251. https://doi.org/10.1016/j.agrformet.2006.07.003

R Core Team (2025) R: A Language and Environment for Statistical Computing

Rahmstorf S, Coumou D (2011) Increase of extreme events in a warming world | PNAS. PNAS 108(44):17905–17909

Rieu I, Twell D, Firon N (2017) Pollen Development at High Temperature: From Acclimation to Collapse. Plant Physiol 173(4):1967–1976. https://doi.org/10.1104/pp.16.01644

Sakata T, Takahashi H, Nishiyama I, Higashitani A (2000) Effects of High Temperature on the Development of Pollen Mother Cells and Microspores in Barley Hordeum vulgare L. J Plant Res 113(4):395–402. https://doi.org/10.1007/PL00013947

Sanders PM, Bui AQ, Weterings K, McIntire KN, Hsu Y-C, Lee PY, Truong MT, Beals TP, Goldberg RB (1999) Anther developmental defects in Arabidopsis thaliana male-sterile mutants. Sex Plant Reprod 11(6):297–322. https://doi.org/10.1007/s004970050158

Schindelin J, Arganda-Carreras I, Frise E, Kaynig V, Longair M, Pietzsch T, Preibisch S, Rueden C, Saalfeld S, Schmid B, Tinevez J-Y, White DJ, Hartenstein V, Eliceiri K, Tomancak P, Cardona A (2012) Fiji: an open-source platform for biological-image analysis. Nat Methods 9(7):676–682. https://doi.org/10.1038/nmeth.2019

Sevillano V, Aznarte JL (2018) Improving classification of pollen grain images of the POLEN23E dataset through three different applications of deep learning convolutional neural networks. PLOS ONE 13(9):e0201807. https://doi.org/10.1371/journal.pone.0201807

Smyth DR, Bowman JL, Meyerowitz EM (1990) Early flower development in Arabidopsis. Plant Cell 2(8):755–767. https://doi.org/10.1105/tpc.2.8.755

Song G, Wang M, Zeng B, Zhang J, Jiang C, Hu Q, Geng G, Tang C (2015) Anther response to high-temperature stress during development and pollen thermotolerance heterosis as revealed by pollen tube growth and in vitro pollen vigor analysis in upland cotton. Planta 241(5):1271–1285. https://doi.org/10.1007/s00425-015-2259-7

Stringer C, Wang T, Michaelos M, Pachitariu M (2021) Cellpose: a generalist algorithm for cellular segmentation. Nat Methods 18(1):100–106. https://doi.org/10.1038/s41592-020-01018-x

Tabas-Madrid D, Méndez-Vigo B, Arteaga N, Marcer A, Pascual-Montano A, Weigel D, Xavier Picó F, Alonso-Blanco C (2018) Genome-wide signatures of flowering adaptation to climate temperature: Regional analyses in a highly diverse native range of Arabidopsis thaliana. Plant Cell Environ 41(8):1806–1820. https://doi.org/10.1111/pce.13189

Turner SD (2014) qqman: an R package for visualizing GWAS results using Q-Q and manhattan plots. 005165

Wahid A, Gelani S, Ashraf M, Foolad MR (2007) Heat tolerance in plants: An overview. Environ Exp Bot 61(3):199–223. https://doi.org/10.1016/j.envexpbot.2007.05.011

Warner RM, Erwin JE (2005) Naturally occurring variation in high temperature induced floral bud abortion across Arabidopsis thaliana accessions. Plant Cell Environ 28(10):1255–1266. https://doi.org/10.1111/j.1365-3040.2005.01361.x

Wiese AJ, Torutaeva E, Honys D (2024) The transcription factors and pathways underpinning male reproductive development in Arabidopsis. Front Plant Sci 15. https://doi.org/10.3389/fpls.2024.1354418

Wu C, Cui K, Li Q, Li L, Wang W, Hu Q, Ding Y, Li G, Fahad S, Huang J, Nie L, Peng S (2021) Estimating the yield stability of heat-tolerant rice genotypes under various heat conditions across reproductive stages: a 5-year case study. Sci Rep 11(1):13604. https://doi.org/10.1038/s41598-021-93079-x

Xiao Y, Pan Y, Luo L, Deng H, Zhang G, Tang W, Chen L (2011) Quantitative Trait Loci Associated with Pollen Fertility under High Temperature Stress at Flowering Stage in Rice (*Oryza sativa*). Rice Sci 18(3):204–209. https://doi.org/10.1016/S1672-6308(11)60028-0

Xu J, Jansma SY, Wolters-Arts M, de Groot PFM, Jansen MJ, Rieu I (2022) Long-Term Mild Heat Causes Post-Mitotic Pollen Abortion Through a Local Effect on Flowers. Front Plant Sci 13. https://doi.org/10.3389/fpls.2022.925754

Xu J, Wolters-Arts M, Mariani C, Huber H, Rieu I (2017) Heat stress affects vegetative and reproductive performance and trait correlations in tomato (Solanum lycopersicum). Euphytica 213(7):156. https://doi.org/10.1007/s10681-017-1949-6

Yamaguchi A, Kobayashi Y, Goto K, Abe M, Araki T (2005) TWIN SISTER OF FT (TSF) Acts as a Floral Pathway Integrator Redundantly with FT. Plant Cell Physiol 46(8):1175–1189. https://doi.org/10.1093/pcp/pci151

Yamamoto M, Uji S, Sugiyama T, Sakamoto T, Kimura S, Endo T, Nishikawa S (2020) ERdj3B-Mediated Quality Control Maintains Anther Development at High Temperatures1 [OPEN]. Plant Physiol 182(4):1979–1990. https://doi.org/10.1104/pp.19.01356

Zhang N, Belsterling B, Raszewski J, Tonsor SJ (2015) Natural populations of Arabidopsis thaliana differ in seedling responses to high-temperature stress. AoB PLANTS 7:plv101. https://doi.org/10.1093/aobpla/plv101

Supplementary Material

Table S1 Accessions of Iberian+ diversity panel. Shown is accession name, first published source, alternate and full name, country of origin, longitude and latitude of collection area in degrees, elevation of collection area in meters, vernalization period in days, and mean pollen viability (PV), early heat tolerance (EHT) and late heat tolerance (LHT) with standard deviation, and mean flowering time (FT) as determined in this study

Accession	Source	Alternate name	Full name	Country	Longitude	Latitude	Elevation	Vern[1]	PV[2]	EHT[3]	LHT[4]	FT[5]
Aul0	Arteaga et al., 2021	IP-Aul-0	Aulencia	Spain	-4.019	40.519	835.34	49	63.9 ± 19.6	95.9 ± 3.9	67.2 ± 17.6	74
Bes5	Arteaga et al., 2021	IP-Bes-5	Besande	Spain	-4.915	42.909	1271.97	49	87.0 ± 0.4	99.1 ± 0.0	88.3 ± 0.1	95
Bor0	Arteaga et al., 2021	IP-Bor-0	Borrenes	Spain	-6.708	42.491	705.96	49	81.0 ± 6.4	91.2 ± 4.5	89.6 ± 6.2	71
Cas0	Arteaga et al., 2021	IP-Cas-0	Castellar de Santiago	Spain	-3.391	38.534	817.15	49	78.6 ± 11.3	98.1 ± 1.5	80.1 ± 11.3	74
Cat0	Arteaga et al., 2021	IP-Cat-0	Cantoblanco	Spain	-3.687	40.542	670.01	49	75.9 ± 2.6	93.6 ± 0.3	81.2 ± 2.8	76
Cir0	Arteaga et al., 2021	IP-Cir-0	Ciudad Rodrigo	Spain	-6.571	40.608	708.69	49	50.3 ± 35.7	85.4 ± 19.3	55.7 ± 31.2	71
Cod0	Arteaga et al., 2021	IP-Cod-0	Codos	Spain	-1.317	41.253	936.66	35	77.7 ± 13.5	96.5 ± 3.7	79.8 ± 12.0	69
Con0	Arteaga et al., 2021	IP-Con-0	Constantina	Spain	-5.599	37.938	631.50	49	50.8 ± 16.0	91.2 ± 11.0	54.8 ± 9.8	73
Coy0	Arteaga et al., 2021	IP-Coy-0	Colmenar del Arroyo	Spain	-4.267	40.442	840.24	35	56.5 ± 37.7	90.3 ± 7.6	63.9 ± 33.4	68
Dar0	Arteaga et al., 2021	IP-Dar-0	Daroca	Spain	-1.432	41.129	843.85	49	63.8 ± 12.4	88.9 ± 10.3	72.3 ± 5.8	74
Elp0	Arteaga et al., 2021	IP-Elp-0	El Pinar de las Rozas	Spain	-3.918	40.526	755.25	35	20.4 ± 28.0	38.7 ± 47.9	59.2 ± 6.7	69
Esn2	Arteaga et al., 2021	IP-Esn-2	Escanilla	Spain	0.192	42.270	682.33	49	40.9 ± NA	63.8 ± NA	65.3 ± NA	77
Evs0	Arteaga et al., 2021	IP-Evs-0	Ermita Virgen del Soto	Spain	-3.960	40.479	639.00	49	51.0 ± 14.2	85.2 ± 12.1	61.1 ± 11.9	72
Lac0	Arteaga et al., 2021	IP-Lac-0	Las Caldas	Spain	-5.916	43.324	223.26	28	53.5 ± 34.3	92.2 ± 13.9	56.6 ± 32.5	58
Laf1	Arteaga et al., 2021	IP-Laf-1	La Frialdad	Spain	-5.883	43.360	262.06	49	70.8 ± 1.7	98.9 ± 1.0	71.3 ± 1.1	72
Lch0	Arteaga et al., 2021	IP-Lch-0	La Chaparrita	Spain	-4.001	40.507	835.34	49	62.5 ± 3.9	90.0 ± 2.4	70.9 ± 2.2	72
Loz0	Arteaga et al., 2021	IP-Loz-0	Lozoya	Spain	-3.801	40.978	1484.65	49	49.1 ± 32.0	87.7 ± 16.6	55.4 ± 29.8	95
Mat0	Arteaga et al., 2021	IP-Mat-0	Martorell de la Selva	Spain	2.685	41.761	115.64	35	43.7 ± 9.3	95.9 ± 1.2	39.8 ± 14.8	67
Mie1	Arteaga et al., 2021	IP-Mie-1	Mierla	Spain	-3.219	40.942	965.57	49	18.1 ± 21.9	64.2 ± 21.9	36.9 ± 45.6	83
Moe0	Arteaga et al., 2021	IP-Moe-0	Montseny	Spain	2.367	41.779	835.70	35	57.9 ± NA	90.3 ± NA	70.2 ± NA	69
Pad0	Arteaga et al., 2021	IP-Pad-0	Prades	Spain	0.992	41.337	784.76	49	6.7 ± NA	49.2 ± NA	15.5 ± NA	83
Pib1	Arteaga et al., 2021	IP-Pib-1	Pino de Bureba	Spain	-3.439	42.721	775.72	49	63.4 ± 20.6	98.5 ± 1.0	65.2 ± 19.4	81
Pie0	Arteaga et al., 2021	IP-Pie-0	Piedrahita	Spain	-5.325	40.464	1265.77	49	43.4 ± 23.6	82.3 ± 11.3	53.0 ± 21.9	74
Pil0	Arteaga et al., 2021	IP-Pil-0	Pico Almenara	Spain	-4.264	40.454	840.24	35	80.2 ± 5.6	98.1 ± 1.5	82.8 ± 4.8	70
Pru0	Arteaga et al., 2021	IP-Pru-0	Prullans	Spain	1.725	42.379	1328.05	49	33.4 ± 32.7	48.2 ± 25.5	59.4 ± 27.4	73

Pun0	Arteaga et al., 2021	IP-Pun-0	Puente Nueva	Spain	-4.776	40.403	1053.57	49	65.4 ± 28.4	95.3 ± 6.9	67.3 ± 27.4	72
Pva1	Arteaga et al., 2021	IP-Pva-1	Puebla de Valles	Spain	-3.306	40.927	984.42	35	75.6 ± 15.4	96.2 ± 4.8	78.3 ± 12.9	69
Sen0	Arteaga et al., 2021	IP-Sen-0	Senet	Spain	0.763	42.587	1839.98	49	64.1 ± 21.0	93.2 ± 4.1	69.6 ± 20.6	83
Sfb6	Arteaga et al., 2021	IP-Sfb-6	Sant Feliu de Buixalleu	Spain	2.569	41.783	231.94	35	85.5 ± NA	98.7 ± NA	85.3 ± NA	69
Som0	Arteaga et al., 2021	IP-Som-0	Somosierra	Spain	-3.580	41.138	1544.49	49	64.7 ± 17.8	94.3 ± 3.9	69.8 ± 21.3	88
Usa0	Arteaga et al., 2021	IP-Usa-0	Usanos	Spain	-3.246	40.710	787.33	49	69.1 ± 5.2	97.2 ± 2.2	70.8 ± 4.3	78
Adc5	Arteaga et al., 2021	IP-Adc-5	Argamasilla de Calatrava	Spain	-4.073	38.765	701.45	35	60.9 ± 29.2	79.9 ± 32.8	77.2 ± 16.5	70
Adm0	Arteaga et al., 2021	IP-Adm-0	Arroba de los Montes	Spain	-4.544	39.145	670.32	49	42.5 ± 9.0	80.6 ± 9.6	54.1 ± 4.0	73
Ara4	Arteaga et al., 2021	IP-Ara-4	Aranda de Duero	Spain	-3.683	41.701	865.22	49	51.6 ± 44.0	93.3 ± 8.1	55.1 ± 41.5	90
Bar1	Arteaga et al., 2021	IP-Bar-1	Barcelona	Spain	2.130	41.433	132.20	49	18.0 ± 15.8	53.1 ± 30.0	33.5 ± 11.2	74
Bdm0	Arteaga et al., 2021	IP-Bdm-0	Bola del Mundo	Spain	-3.991	40.784	1401.49	49	73.5 ± 26.4	97.2 ± 1.9	75.4 ± 27.5	92
Ben0	Arteaga et al., 2021	IP-Ben-0	Benatae	Spain	-2.656	38.371	893.61	49	7.0 ± 6.5	17.8 ± 10.7	37.7 ± 6.2	75
Bis0	Arteaga et al., 2021	IP-Bis-0	Bisaurri	Spain	0.535	42.489	1535.68	49	64.1 ± 8.6	87.9 ± 7.5	75.4 ± 16.7	85
Boa0	Arteaga et al., 2021	IP-Boa-0	Boadilla del Monte	Spain	-3.881	40.396	670.12	35	78.0 ± 18.8	99.2 ± 1.2	79.6 ± 17.5	70
Bra0	Arteaga et al., 2021	IP-Bra-0	Brazuelo	Spain	-6.151	42.495	919.92	49	50.9 ± 17.6	84.3 ± 12.0	60.1 ± 13.5	75
Cab3	Arteaga et al., 2021	IP-Cab-3	Cabrera de Mar	Spain	2.387	41.538	215.97	35	28.7 ± NA	97.0 ± NA	27.2 ± NA	67
Cad0	Arteaga et al., 2021	IP-Cad-0	Candelario	Spain	-5.742	40.365	1523.65	49	57.5 ± 33.3	67.7 ± 37.7	89.2 ± 4.7	78
Cal0	Arteaga et al., 2021	IP-Cal-0	Calamocha	Spain	-1.370	40.941	978.21	49	38.2 ± 23.2	79.7 ± 10.2	47.4 ± 23.7	85
Cap1	Arteaga et al., 2021	IP-Cap-1	Capileira	Spain	-3.360	36.968	1519.19	49	79.6 ± 17.8	97.4 ± 4.6	80.8 ± 14.8	74
Cdc3	Arteaga et al., 2021	IP-Cdc-3	Ciruelos de Coca	Spain	-4.546	41.214	763.28	49	66.0 ± 2.2	96.6 ± 2.6	66.4 ± 0.2	78
Cdo0	Arteaga et al., 2021	IP-Cdo-0	Castrillejos de la Olma	Spain	-4.638	42.231	803.25	49	26.2 ± 26.1	76.7 ± 28.8	31.6 ± 26.3	88
Cem0	Arteaga et al., 2021	IP-Cem-0	Carbonero el Mayor	Spain	-4.317	41.148	845.67	49	57.5 ± 18.3	85.9 ± 7.5	66.9 ± 18.8	76
Cho0	Arteaga et al., 2021	IP-Cho-0	La Chopera de las Rozas	Spain	-3.898	40.513	686.22	35	60.3 ± 28.8	84.0 ± 15.8	68.3 ± 30.6	70
Cmo3	Arteaga et al., 2021	IP-Cmo-3	Cardiel de los Montes	Spain	-4.652	40.049	408.38	35	34.6 ± 21.8	94.6 ± 2.5	35.2 ± 23.7	67
Cot0	Arteaga et al., 2021	IP-Cot-0	Cotanes del Monte	Spain	-5.380	41.827	703.32	35	64.9 ± 4.6	96.4 ± 3.3	65.0 ± 3.8	67
Cum1	Arteaga et al., 2021	IP-Cum-1	Cumbres Mayores	Spain	-6.658	38.067	589.51	35	58.4 ± 34.4	83.1 ± 27.0	65.4 ± 27.1	67
Cur4	Arteaga et al., 2021	IP-Cur-4	Curtis	Spain	-8.093	43.123	493.13	49	53.0 ± 29.7	80.5 ± 16.0	62.4 ± 28.0	75
Ees0	Arteaga et al., 2021	IP-Ees-0	San Lorenzo del Escorial	Spain	-4.147	40.588	967.38	49	64.7 ± 17.4	90.6 ± 10.3	71.7 ± 12.8	73
Elb0	Arteaga et al., 2021	IP-Elb-0	El Brull	Spain	2.339	41.810	896.25	49	75.5 ± 15.4	93.9 ± 8.3	80.2 ± 9.6	78
Ezc2	Arteaga et al., 2021	IP-Ezc-2	Ezcaray	Spain	-3.026	42.305	1049.17	49	82.0 ± 13.0	94.4 ± 5.9	85.7 ± 9.5	86

Fue2	Arteaga et al., 2021	IP-Fue-2	Fuente Obejuna	Spain	-5.425	38.262	606.67	35	59.5 ± 28.5	76.8 ± 15.5	77.3 ± 19.5	70
Glo1	Arteaga et al., 2021	IP-Glo-1	Garganta de la Olla	Spain	-5.776	40.111	1060.93	49	29.3 ± 20.4	81.5 ± 9.1	37.0 ± 23.3	75
Gra0	Arteaga et al., 2021	IP-Gra-0	Grazalema	Spain	-5.395	36.768	930.83	49	56.5 ± 23.0	97.1 ± 1.6	58.1 ± 23.1	74
Gua1	Arteaga et al., 2021	IP-Gua-1	Guadalupe	Spain	-5.336	39.399	588.69	35	65.7 ± 19.9	91.4 ± 6.6	71.2 ± 18.6	68
Her12	Arteaga et al., 2021	IP-Her-12	Herguijuela	Spain	-5.783	39.395	516.94	35	54.6 ± 31.7	96.3 ± 3.7	57.3 ± 31.7	70
Hom4	Arteaga et al., 2021	IP-Hom-4	Hombrados	Spain	-1.686	40.817	1190.38	49	34.4 ± 35.1	62.2 ± 24.4	52.4 ± 36.9	92
Hue3	Arteaga et al., 2021	IP-Hue-3	Huergas de Babia	Spain	-6.106	42.956	1499.22	49	70.5 ± 20.0	98.4 ± 1.5	72.8 ± 20.4	95
Hum2	Arteaga et al., 2021	IP-Hum-2	Humienta	Spain	-3.689	42.227	931.21	49	69.9 ± 24.0	98.9 ± 0.3	71.8 ± 23.8	75
Ini0	Arteaga et al., 2021	IP-Ini-0	Madrid-INIA	Spain	-3.748	40.454	637.00	49	74.3 ± 21.7	97.3 ± 1.9	75.7 ± 21.3	71
Lab7	Arteaga et al., 2021	IP-Lab-7	Labajos	Spain	-4.498	40.866	1016.95	49	60.7 ± 14.3	98.8 ± 1.3	60.0 ± 17.2	83
Lam0	Arteaga et al., 2021	IP-Lam-0	Las Matas	Spain	-3.889	40.567	686.22	35	79.4 ± 8.2	96.0 ± 3.2	83.2 ± 6.8	70
Ldd0	Arteaga et al., 2021	IP-Ldd-0	Laguna de Duero	Spain	-4.707	41.576	692.09	49	45.5 ± 46.9	53.2 ± 52.6	77.8 ± 13.3	80
Lro0	Arteaga et al., 2021	IP-Lro-0	Las Rozas	Spain	-3.878	40.496	688.27	49	73.7 ± 24.1	89.1 ± 16.1	81.5 ± 14.9	71
Lso0	Arteaga et al., 2021	IP-Lso-0	La Solana	Spain	-3.163	38.858	781.66	49	55.5 ± 12.6	95.4 ± 1.8	59.2 ± 13.1	77
Lum0	Arteaga et al., 2021	IP-Lum-0	Lumbreras	Spain	-2.622	42.238	1070.61	49	67.4 ± 10.2	97.2 ± 1.2	68.8 ± 9.4	76
Mad0	Arteaga et al., 2021	IP-Mad-0	Madrid-Centro	Spain	-3.674	40.445	668.36	35	72.5 ± 28.5	98.3 ± 1.8	72.1 ± 29.0	68
Mdd0	Arteaga et al., 2021	IP-Mdd-0	Molinos de Duero	Spain	-2.788	41.887	1101.59	49	61.3 ± 2.9	98.1 ± 0.1	61.0 ± 0.9	95
Men2	Arteaga et al., 2021	IP-Men-2	Menasalbas	Spain	-4.345	39.658	709.56	49	73.9 ± 2.9	96.4 ± 1.0	76.8 ± 3.4	74
Moa0	Arteaga et al., 2021	IP-Moa-0	Montanuy	Spain	0.698	42.462	1306.81	49	48.3 ± 31.1	80.0 ± 16.5	57.7 ± 28.4	96
Moc11	Arteaga et al., 2021	IP-Moc-11	Molacillos	Spain	-5.641	41.565	640.23	49	23.7 ± 11.5	51.0 ± 31.4	49.3 ± 13.5	71
Mon5	Arteaga et al., 2021	IP-Mon-5	Montoro	Spain	-4.384	38.059	253.54	35	20.0 ± 15.2	67.9 ± 15.9	28.6 ± 13.3	70
Mos1	Arteaga et al., 2021	IP-Mos-1	Monsanto	Portugal	-7.110	40.041	438.99	49	21.7 ± NA	86.1 ± NA	27.5 ± NA	71
Mur0	Arteaga et al., 2021	IP-Mur-0	Mura	Spain	1.999	41.674	607.66	49	72.5 ± 13.9	95.0 ± 6.8	77.1 ± 17.1	84
Nac0	Arteaga et al., 2021	IP-Nac-0	Navacerrada	Spain	-3.994	40.751	1401.49	49	63.4 ± 14.7	92.4 ± 3.6	70.6 ± 17.4	83
Nog17	Arteaga et al., 2021	IP-Nog-17	Noguera	Spain	-1.601	40.451	1605.06	49	66.2 ± 45.0	98.6 ± 1.5	66.5 ± 45.8	99
Oja0	Arteaga et al., 2021	IP-Oja-0	Ojacastro	Spain	-2.997	42.344	1023.65	35	33.1 ± 8.1	91.0 ± 10.6	35.9 ± 2.0	68
Orb10	Arteaga et al., 2021	IP-Orb-10	Orbaitzeta	Spain	-1.230	42.972	957.44	49	40.1 ± 8.2	75.6 ± 10.5	55.0 ± 4.9	74
Oso0	Arteaga et al., 2021	IP-Oso-0	Osorno	Spain	-4.361	42.443	835.83	49	25.5 ± 19.2	58.4 ± 12.8	47.3 ± 29.7	88
Ovi1	Arteaga et al., 2021	IP-Ovi-1	Oviedo	Spain	-5.867	43.380	262.06	28	38.8 ± 11.0	78.0 ± 20.4	52.3 ± 1.5	58
Pan0	Arteaga et al., 2021	IP-Pan-0	Balneario de Panticosa	Spain	-0.232	42.760	2164.65	49	35.1 ± 26.2	74.1 ± 12.9	45.4 ± 27.2	85

Pds1	Arteaga et al., 2021	IP-Pds-1	Palacios del Sil	Spain	-6.450	42.873	1188.45	49	91.1 ± 0.4	99.8 ± 0.1	91.7 ± 0.7	76
Ped0	Arteaga et al., 2021	IP-Ped-0	La Pedriza	Spain	-3.898	40.738	1116.32	49	82.1 ± 15.4	97.9 ± 1.4	84.0 ± 14.2	74
Piq0	Arteaga et al., 2021	IP-Piq-0	Piqueras	Spain	-2.564	42.096	1522.92	35	37.5 ± 24.0	93.8 ± 3.7	39.0 ± 24.5	69
Pro0	Arteaga et al., 2021	IP-Pro-0	Proaza	Spain	-6.012	43.277	675.26	28	68.5 ± 14.0	95.3 ± 6.6	71.8 ± 9.3	58
Pub0	Arteaga et al., 2021	IP-Pub-0	Puebla de Sanabria	Spain	-6.633	42.057	976.44	49	61.7 ± 16.9	81.0 ± 12.1	75.6 ± 10.5	73
Qui-0	Arteaga et al., 2021	IP-Qui-0	Quintela	Spain	-6.930	42.692	878.23	35	78.3 ± 11.3	96.4 ± 5.3	81.3 ± 7.3	68
Reg0	Arteaga et al., 2021	IP-Reg-0	Reguengo	Portugal	-7.402	39.287	377.31	35	72.8 ± 9.9	94.5 ± 3.3	77.8 ± 8.3	67
Rei0	Arteaga et al., 2021	IP-Rei-0	Reliquias	Portugal	-7.595	38.745	363.53	35	22.6 ± 14.9	72.7 ± 31.8	32.3 ± 8.6	67
Rel0	Arteaga et al., 2021	IP-Rel-0	Relumbrar	Spain	-2.705	38.602	940.69	49	5.1 ± 0.6	39.7 ± 14.6	14.0 ± 4.4	76
San10	Arteaga et al., 2021	IP-San-10	Santa Elena	Spain	-3.509	38.331	717.81	49	52.8 ± 28.9	74.9 ± 19.9	70.4 ± 21.6	71
Sdv3	Arteaga et al., 2021	IP-Sdv-3	Santa Olaja de Varga	Spain	-5.123	42.836	1182.19	49	30.3 ± 6.2	84.4 ± 13.1	36.6 ± 14.5	89
Ses0	Arteaga et al., 2021	IP-Ses-0	Sestrica	Spain	-1.632	41.484	814.25	49	4.7 ± 3.7	43.3 ± 23.6	12.3 ± 1.4	76
Smt1	Arteaga et al., 2021	IP-Smt-1	Santa Marta de Tormes	Spain	-5.635	40.951	802.54	49	87.8 ± 0.3	98.6 ± 1.4	89.2 ± 1.2	71
Sne0	Arteaga et al., 2021	IP-Sne-0	Sierra Nevada	Spain	-3.262	37.075	2388.22	49	76.4 ± 24.0	89.1 ± 16.9	84.5 ± 13.2	85
Svi0	Arteaga et al., 2021	IP-Svi-0	San Vicente	Spain	-7.396	43.396	544.36	28	75.3 ± 9.1	92.5 ± 2.7	80.0 ± 8.4	53
Toe0	Arteaga et al., 2021	IP-Toe-0	Torrelodones	Spain	-3.915	40.593	755.25	49	68.7 ± 23.8	94.6 ± 5.1	74.2 ± 21.8	76
Tol7	Arteaga et al., 2021	IP-Tol-7	Tolva	Spain	0.594	42.109	808.94	49	51.9 ± NA	93.9 ± NA	55.7 ± NA	83
Tor1	Arteaga et al., 2021	IP-Tor-1	Torreandaluz	Spain	-2.836	41.595	948.78	49	48.0 ± 11.7	78.1 ± 4.2	61.0 ± 11.1	77
Trs0	Arteaga et al., 2021	IP-Trs-0	Tresali	Spain	-5.493	43.364	383.10	28	75.2 ± 1.8	90.2 ± 9.3	80.7 ± 12.2	53
Urd1	Arteaga et al., 2021	IP-Urd-1	Urdanta	Spain	-2.984	42.273	1538.63	49	77.4 ± 18.2	98.6 ± 1.8	77.5 ± 18.7	92
Vad0	Arteaga et al., 2021	IP-Vad-0	Valdenoceda	Spain	-3.592	42.858	793.73	35	69.6 ± 18.4	99.0 ± 1.1	70.5 ± 18.3	67
Vav0	Arteaga et al., 2021	IP-Vav-0	Valverde	Portugal	-8.019	38.532	272.35	35	45.8 ± 49.6	74.5 ± 35.0	53.1 ± 40.3	67
Vaz0	Arteaga et al., 2021	IP-Vaz-0	Valdezcaray	Spain	-2.989	42.260	1538.63	49	53.8 ± 28.3	83.9 ± 14.5	63.4 ± 25.1	88
Vdt0	Arteaga et al., 2021	IP-Vdt-0	Villagonzalo de Tormes	Spain	-5.496	40.890	832.42	49	28.4 ± 14.5	69.4 ± 12.4	40.0 ± 14.9	75
Ven0	Arteaga et al., 2021	IP-Ven-0	El Ventorrillo	Spain	-4.014	40.758	1403.38	49	66.4 ± 10.2	97.3 ± 2.8	68.0 ± 7.4	76
Vid1	Arteaga et al., 2021	IP-Vid-1	Vidigueira	Portugal	-7.845	38.224	236.62	28	63.2 ± 19.4	93.0 ± 5.8	66.7 ± 21.5	53
Vie-0	Arteaga et al., 2021	IP-Vie-0	Vielha	Spain	0.763	42.627	1989.71	49	60.4 ± 26.6	82.6 ± 19.7	71.6 ± 18.7	83
Vig1	Arteaga et al., 2021	IP-Vig-1	Viguera	Spain	-2.531	42.308	746.40	35	61.5 ± 19.7	97.2 ± 1.1	63.6 ± 20.4	70
Vim0	Arteaga et al., 2021	IP-Vim-0	Villarino de Manzanas	Spain	-6.510	41.877	737.63	49	67.2 ± 26.0	98.2 ± 2.8	67.7 ± 26.6	73
Vis0	Arteaga et al., 2021	IP-Vis-0	Villareal de San Carlos	Spain	-6.045	39.846	326.65	35	64.6 ± 12.0	96.3 ± 1.8	67.3 ± 13.6	67

Vpa1	Arteaga et al., 2021	IP-Vpa-1	Villanueva del Pardillo	Spain	-3.966	40.494	639.00	35	61.1 ± NA	89.9 ± NA	69.7 ± NA	70
Zar0	Arteaga et al., 2021	IP-Zar-0	Zarzalejo	Spain	-4.195	40.552	967.38	49	70.1 ± 26.0	94.1 ± 10.5	72.3 ± 21.1	82
Bab-0	Durvasula et al. 2017			Morocco	-5.024	35.043	963.17	49	54.5 ± 31.3	85.3 ± 9.7	63.2 ± 27.9	78
Taz-0	Durvasula et al. 2017			Morocco	-4.103	34.092	1382.58	49	31.2 ± 20.5	86.5 ± 11.3	33.9 ± 19.9	75
Tah-0	Durvasula et al. 2017			Morocco	-4.222	34.053	959.46	49	78.8 ± 13.8	96.2 ± 1.1	82.9 ± 11.9	71
Bba-2	Durvasula et al. 2017			Morocco	-4.084	34.019	1374.96	35	67.7 ± 13.2	90.0 ± 1.2	72.9 ± 10.4	68
Tiz-0	Durvasula et al. 2017			Morocco	-4.026	33.872	1470.33	49	65.4 ± 26.1	93.4 ± 6.1	67.6 ± 26.5	81
Azr-0	Durvasula et al. 2017			Morocco	-5.179	33.424	1686.59	49	71.9 ± 5.7	93.9 ± 4.7	77.2 ± 4.2	74
Agl-0	Durvasula et al. 2017			Morocco	-5.449	32.972	1598.22	35	69.1 ± 26.4	98.6 ± 0.2	70.7 ± 26.4	69
Khe-0	Durvasula et al. 2017			Morocco	-5.510	32.927	1323.34	35	65.0 ± 15.0	94.2 ± 3.7	69.2 ± 12.9	70
Elk-1	Durvasula et al. 2017			Morocco	-6.015	32.535	1167.03	35	31.3 ± 33.9	77.6 ± 15.8	37.4 ± 37.1	69
Oua-0	Durvasula et al. 2017			Morocco	-6.275	32.079	1549.75	49	60.7 ± 18.2	97.1 ± 2.2	60.6 ± 19.1	73
Til-2	Durvasula et al. 2017			Morocco	-6.230	32.042	1549.75	35	75.5 ± 11.3	94.3 ± 7.0	79.6 ± 6.3	69
Elh-2	Durvasula et al. 2017			Morocco	-7.406	31.472	1619.98	35	68.4 ± 7.0	95.5 ± 1.7	70.9 ± 5.7	69
Set-0	Durvasula et al. 2017			Morocco	-7.674	31.227	2037.53	35	34.1 ± 24.2	68.1 ± 16.3	50.3 ± 30.0	69
Bad1	Arteaga et al., 2021	IP-Bad-1	Barbadaes de Cima	Portugal	-7.555	41.569	854.76	49	64.3 ± 17.9	93.5 ± 9.1	68.9 ± 13.4	73
Cai3	Arteaga et al., 2021	IP-Cai-3	Canencia	Spain	-3.764	40.868	1300.64	49	16.8 ± 17.3	99.5 ± 0.7	14.9 ± 14.3	101
Cdr0	Arteaga et al., 2021	IP-Cdr-0	Caldas de Reis	Spain	-8.652	42.601	178.75	35	40.2 ± 15.5	81.9 ± 6.7	47.9 ± 16.6	70
Cib0	Arteaga et al., 2021	IP-Cib-0	Cibanal	Spain	-6.328	41.276	705.54	49	76.0 ± 23.0	92.4 ± 8.8	80.0 ± 18.2	78
Fot1	Arteaga et al., 2021	IP-Fot-1	Fontanosas	Spain	-4.520	38.770	605.90	49	39.4 ± 28.4	82.9 ± 9.0	46.6 ± 30.0	74
Frg1	Arteaga et al., 2021	IP-Frg-1	Freginals	Spain	0.510	40.674	156.09	49	56.7 ± 24.5	94.1 ± 8.4	60.8 ± 23.0	71
Gdm8	Arteaga et al., 2021	IP-Gdm-8	Granja de Moreruela	Spain	-5.783	41.846	703.40	49	87.3 ± 7.4	98.9 ± 0.7	88.5 ± 6.8	81
Grs0	Arteaga et al., 2021	IP-Grs-0	Grandas de Salime	Spain	-6.849	43.238	527.58	35	11.4 ± NA	89.2 ± NA	13.5 ± NA	68
JalC3	Arteaga et al., 2021	IP-JalC-3	Jalance	Spain	-1.145	39.229	649.68	49	82.3 ± 14.3	98.5 ± 1.1	84.0 ± 13.1	76
Las0	Arteaga et al., 2021	IP-Las-0	La Silla de Felipe II	Spain	-4.153	40.568	967.38	49	49.0 ± 20.5	94.1 ± 3.6	52.6 ± 20.7	78
Lbe4	Arteaga et al., 2021	IP-Lbe-4	La Berzosa	Spain	-3.930	40.601	1007.88	49	73.0 ± 14.3	97.2 ± 2.1	75.0 ± 14.5	78
Lhi4	Arteaga et al., 2021	IP-Lhi-4	La Hiruela	Spain	-3.459	41.073	1375.80	49	71.1 ± 14.6	97.5 ± 1.3	73.1 ± 14.1	92
Liz0	Arteaga et al., 2021	IP-Liz-0	Lizartza	Spain	-2.034	43.100	303.39	49	57.7 ± 27.9	83.9 ± 29.0	68.1 ± 16.2	71
Lor0	Arteaga et al., 2021	IP-Lor-0	Lorcha	Spain	-0.263	38.860	478.08	49	77.8 ± 16.7	95.4 ± 1.6	82.8 ± 14.3	78
Lta0	Arteaga et al., 2021	IP-Lta-0	Los Tanagos	Spain	-4.440	43.380	149.28	35	11.4 ± NA	40.5 ± NA	31.2 ± NA	70

Mag0	Arteaga et al., 2021	IP-Mag-0	Mangualde	Portugal	-7.753	40.624	459.65	35	29.6 ± 34.6	79.4 ± 7.7	36.4 ± 43.5	68
Mal0	Arteaga et al., 2021	IP-Mal-0	Malaguilla	Spain	-3.287	40.841	868.18	49	53.4 ± 22.1	86.0 ± 10.4	61.1 ± 20.3	76
Mdc0	Arteaga et al., 2021	IP-Mdc-0	Moral de Calatrava	Spain	-3.530	38.874	750.51	49	64.3 ± 17.4	95.6 ± 0.5	66.6 ± 17.4	74
Mor0	Arteaga et al., 2021	IP-Mor-0	Moral de Castro	Spain	-6.073	40.870	796.13	49	71.1 ± 17.4	96.6 ± 3.0	74.2 ± 17.3	75
Mra7	Arteaga et al., 2021	IP-Mra-7	Mora	Spain	-3.636	39.670	688.95	49	78.3 ± 14.4	98.1 ± 1.8	80.5 ± 14.4	75
Nat8	Arteaga et al., 2021	IP-Nat-8	Navaltoril	Spain	-4.763	39.574	859.09	49	42.5 ± 43.9	83.8 ± 15.2	46.7 ± 42.3	74
Nav1	Arteaga et al., 2021	IP-Nav-1	Navaluenga	Spain	-4.647	40.418	933.04	35	58.7 ± 25.5	94.6 ± 3.0	64.1 ± 23.0	70
Ndr3	Arteaga et al., 2021	IP-Ndr-3	Nava de Roa	Spain	-4.006	41.611	853.48	49	49.6 ± 4.3	98.6 ± 0.7	49.7 ± 3.7	83
Ola0	Arteaga et al., 2021	IP-Ola-0	Olate	Spain	-2.630	43.049	664.07	49	56.5 ± 19.1	91.8 ± 6.7	60.5 ± 17.2	74
Pto0	Arteaga et al., 2021	IP-Pto-0	La Pobla de Tornesa	Spain	0.010	40.100	291.99	35	48.9 ± 7.5	70.9 ± 13.1	70.2 ± 10.2	70
Puv0	Arteaga et al., 2021	IP-Puv-0	Puerto de Vega	Spain	-6.645	43.565	168.18	35	84.3 ± NA	96.1 ± NA	88.7 ± NA	68
Rob1	Arteaga et al., 2021	IP-Rob-1	Robledillo	Spain	-4.851	39.583	809.13	49	84.0 ± 10.4	97.8 ± 1.3	85.9 ± 8.3	71
Sca0	Arteaga et al., 2021	IP-Sca-0	San Calixto	Spain	-5.370	37.962	409.99	35	71.2 ± 18.4	95.0 ± 4.3	75.4 ± 14.8	68
Slc3	Arteaga et al., 2021	IP-Slc-3	San Lorenzo de Calatrava	Spain	-3.744	38.471	902.08	49	64.4 ± 37.3	92.4 ± 9.6	67.6 ± 34.5	76
Sln22	Arteaga et al., 2021	IP-Sln-22	Sevilla la Nueva	Spain	-3.995	40.357	614.24	49	71.8 ± 7.9	91.3 ± 2.5	78.7 ± 7.0	76
TejB6	Arteaga et al., 2021	IP-TejB-6	Tejerurela	Spain	-2.366	38.397	981.08	49	58.0 ± 33.8	92.8 ± 5.6	61.8 ± 33.0	71
Tod5	Arteaga et al., 2021	IP-Tod-5	Tordesillas	Spain	-5.045	41.468	681.88	49	75.7 ± 20.4	97.8 ± 1.8	78.6 ± 18.1	71
Ura0	Arteaga et al., 2021	IP-Ura-0	Urda	Spain	-3.850	39.423	817.65	35	40.5 ± 17.5	72.3 ± 1.8	54.7 ± 25.3	70
Vai0	Arteaga et al., 2021	IP-Vai-0	Valdigem	Portugal	-7.768	41.131	376.08	35	36.2 ± 30.1	74.0 ± 23.5	49.0 ± 32.8	67
VisB3	Arteaga et al., 2021	IP-VisB-3	Villareal de San Carlos-B	Spain	-6.045	39.846	326.65	35	84.3 ± NA	92.3 ± NA	89.6 ± NA	70
Vlo12	Arteaga et al., 2021	IP-Vlo-1-2	Villarubia de los Ojos	Spain	-3.639	39.284	848.53	49	59.0 ± 35.5	91.8 ± 9.6	62.4 ± 32.8	73

[1]Lon/Lat = longitude and latitude of collection area in degrees; [2]elevation of collection area in meters; [3]Vern = vernalization period in days; [4]PV = mean pollen viability ± standard deviation; [5]EHT = early heat tolerance ± standard deviation; [6]LHT = late heat tolerance ± standard deviation; [7]FT = mean flowering time.

Table S2: Parameters measured for regions-of-interest (ROIs). Full description from ImageJ (https://imagej.net/ij/docs/menus/analyze.html).

Parameter	Description
Area	Area
Perim.	Perimeter
Circ.	Circularity
Round	Roundness
Solidity	Soliditiy
Feret	Feret's diameter: maximum caliper
MinFeret	Feret's diameter: minimum caliper
Ch0_Mean	Channel 0 (Red): Mean gray value of pixels in selection
Ch0_Median	Channel 0 (Red): Median gray value of pixels in selection
Ch0_StdDev	Channel 0 (Red): Standard deviation of pixels in selection
Ch0_IntDen	Channel 0 (Red): Integrated density
Ch0_RawIntDen	Channel 0 (Red): Raw integrated density
Ch0_Skew	Channel 0 (Red): Skewness
Ch0_Kurt	Channel 0 (Red): Kurtosis
Ch1_Mean	Channel 1 (Green): Mean gray value of pixels in selection
Ch1_Median	Channel 1 (Green): Median gray value of pixels in selection
Ch1_StdDev	Channel 1 (Green): Standard deviation gray value of pixels in selection
Ch1_IntDen	Channel 1 (Green): Integrated density
Ch1_RawIntDen	Channel 1 (Green): Raw integrated density
Ch1_Skew	Channel 1 (Green): Skewness
Ch1_Kurt	Channel 1 (Green): Kurtosis
Ch2_Mean	Channel 2 (Blue): Mean gray value of pixels in selection
Ch2_Median	Channel 2 (Blue): Median gray value of pixels in selection
Ch2_StdDev	Channel 2 (Blue): Standard deviation gray value of pixels in selection
Ch2_IntDen	Channel 2 (Blue): Integrated density
Ch2_RawIntDen	Channel 2 (Blue): Raw integrated density
Ch2_Skew	Channel 2 (Blue): Skewness
Ch2_Kurt	Channel 2 (Blue): Kurtosis

Table S3 Pearson's correlation coefficients between geographical and climate variables and pollen viability (PV)

Trait	Elevation	DTR[1]	TG[2]	TX[3]	WM[4]	WQ[5]	WSDI[6]
PV	0.092	0.008	-0.048	-0.025	-0.021	-0.024	0.006

[1]DTR = median of diurnal temperature range; [2]TG = daily mean temperature; [3]TX = maximum of daily maximum temperature; [4]WM = mean temperature of the warmest month; [5]WQ = mean temperature of the warmest quarter; [6]WSDI = warm-spell duration index.

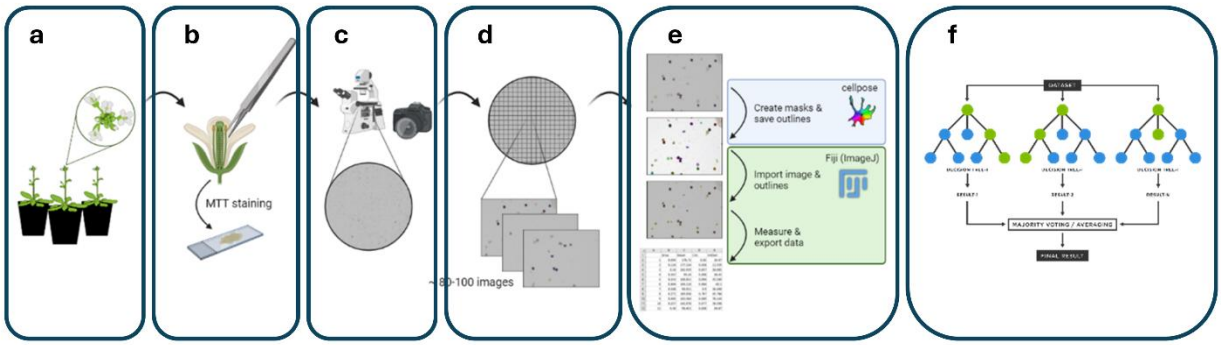

Fig. S1 Graphic visualization of Arabidopsis pollen phenotyping process. A. Arabidopsis plants are grown until flowering stage. B. Flowers at anthesis are sampled and pollen is extracted for differential viability staining with MTT. C. A bright-field microscope equipped with camera is used for high quality image acquisition. D. An image tile scan is obtained for the sample. E. Images are processed for object segmentation and object measurement yielding a spreadsheet containing data for variables differentiating between objects. F. Object classification is done using machine-learning algorithm, generated using a previously obtained train/test-dataset

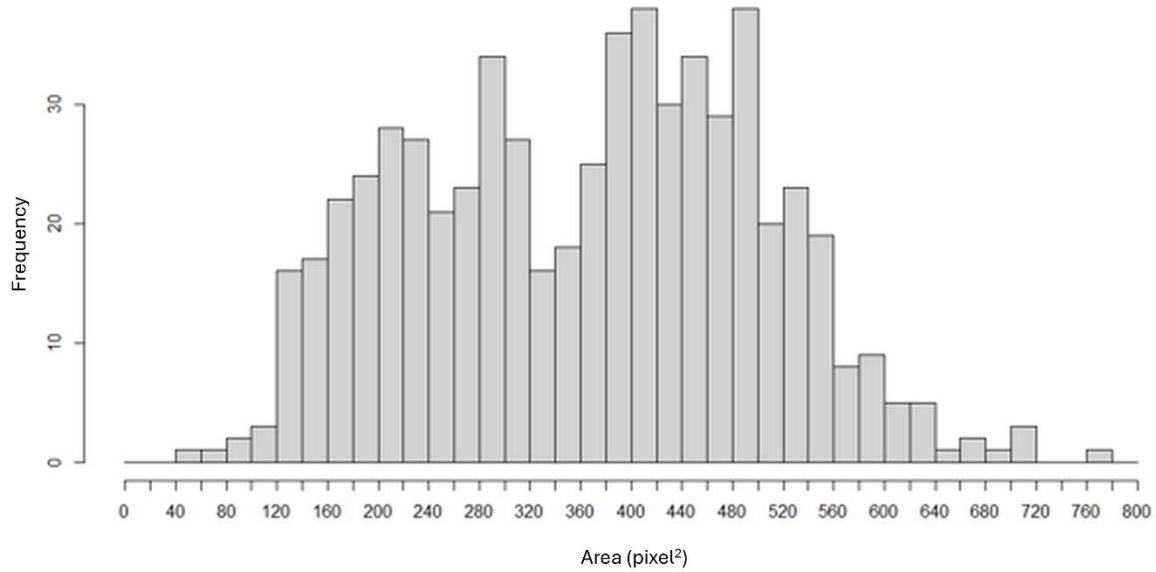

Fig. S2 Histogram of Area value for test/training dataset objects

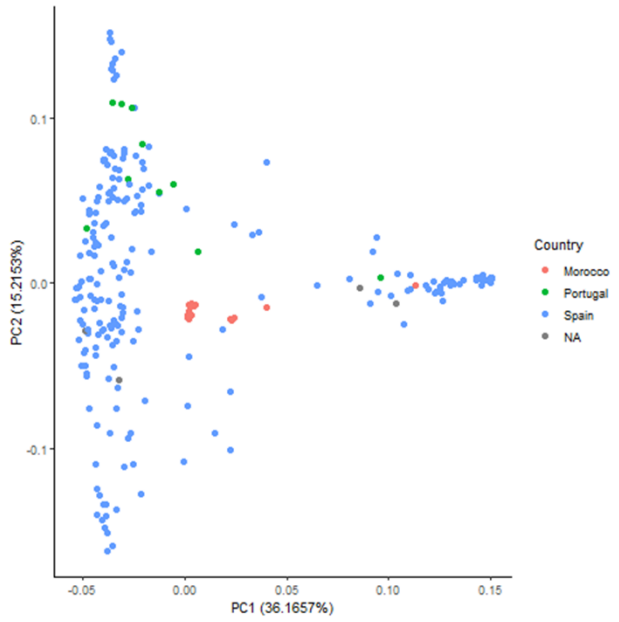

Fig. S3 PCA of the genotypes for the Iberian+ diversity panel. Highlighted are the countries of origin for each of the accessions

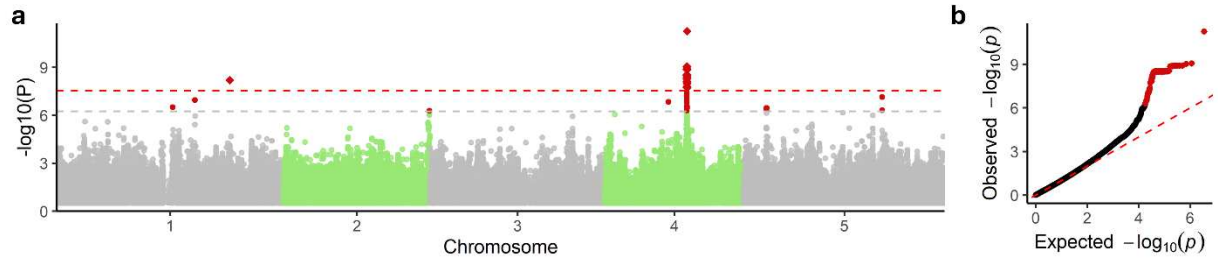

Fig. S4 GWAS results for flowering time for accessions of the Iberian^{+} diversity panel. A, Manhattan plot showing GWAS results for flowering time. Stringent and more lenient significance thresholds are indicated as dashed red and grey lines, respectively. B. Q-Q plot for GWAS results for flowering time. Red dots indicates SNP associated with the trait of interest above the significance threshold